

Low-Dimensional Modelling of Turbulence Using the Proper Orthogonal Decomposition: A Tutorial

TROY R. SMITH¹, JEFF MOEHLIS², and PHILIP HOLMES^{3,*}

¹Control and Dynamical Systems, California Institute of Technology, Mail Stop 107-81, 1200 E. California Blvd, Pasadena, CA 91125, U.S.A.; ²Department of Mechanical and Environmental Engineering, University of California, Santa Barbara, CA 93106, U.S.A.; ³Department of Mechanical and Aerospace Engineering and Program in Applied and Computational Mathematics, Princeton University, Princeton, NJ 08544, U.S.A.; *Author for correspondence (e-mail: pholmes@math.princeton.edu; fax: +1-609-258-6109)

(Received: 6 January 2004; accepted: 22 January 2004)

Abstract. The proper orthogonal decomposition identifies basis functions or modes which optimally capture the average energy content from numerical or experimental data. By projecting the Navier–Stokes equations onto these modes and truncating, one can obtain low-dimensional ordinary differential equation models for fluid flows. In this paper we present a tutorial on the construction of such models. In addition to providing a general overview of the procedure, we describe two different ways to numerically calculate the modes, show how symmetry considerations can be exploited to simplify and understand them, comment on how parameter variations are captured naturally in such models, and describe a generalization of the procedure involving projection onto uncoupled modes that allow streamwise and cross-stream components to evolve independently. We illustrate for the example of plane Couette flow in a minimal flow unit – a domain whose spanwise and streamwise extent is just sufficient to maintain turbulence.

Key words: plane Couette flow, proper orthogonal decomposition, turbulence

1. Introduction

Discussion of low-dimensional modelling of fluid mechanical systems frequently begins with observations regarding the contrast between the complexity of fluid motions and the apparent simplicity of the governing Navier–Stokes equations (hereafter NSE). Indeed, these equations, which for an incompressible, Newtonian fluid may be written in terms of rescaled velocity (\mathbf{u}), pressure (p), density (ρ) and Reynolds number (Re , based on a suitable macroscopic length scale) as

$$\frac{\partial \mathbf{u}}{\partial t} + \mathbf{u} \cdot \nabla \mathbf{u} = -\frac{1}{\rho} \nabla p + \frac{1}{Re} \nabla^2 \mathbf{u}; \quad \nabla \cdot \mathbf{u} = 0, \quad (1)$$

are nothing more than a statement of Newton’s second law in the form, $a = F/m$. The F and m terms which appear on the right-hand side of (1) provide few complications; it is the nonlinear term in the acceleration, appearing on the left-hand side, which causes the majority of the difficulties. Additionally, the continuity equation $\nabla \cdot \mathbf{u} = 0$ leads to the complication of non-locality.

Viewed abstractly as partial differential equations, the NSE have infinitely many degrees of freedom. Furthermore, a Fourier transform of the nonlinear terms in (1) indicates that strong dynamic coupling exists among these ‘modes’. While this is rather discouraging, various results indicate that the situation might not be quite so dire. In particular, classical turbulence theory [47], via dimensional analysis, provides the estimate that the number N of degrees of freedom of a turbulent three-dimensional flow

scales as

$$N \sim \text{Re}^{9/4}. \quad (2)$$

While not completely rigorous, this suggests that the number of degrees of freedom in a turbulent flow (e.g. with Re of the order of 10^4) is a very large, but finite, number.

The relation (2) estimates the number of modes *sufficient* to reliably approximate a turbulent system, but not how many are *necessary*. Clearly the answer to the latter question depends on the flow under consideration. In isotropic, homogeneous turbulence, flow structures display an enormous range of length scales, for example, and thus one might assume that the number of modes indicated by (2) is necessary. In contrast, many flows at lower Reynolds number or in constrained geometries seem to have just a few basic structures which persistently appear, disappear and then appear again. Perhaps the first clear experimental demonstration of these *coherent structures* was in the mixing-layer experiments of [11]. Some years earlier, an unbiased technique for determining which modes, when suitably combined, can form such structures was proposed in [33]. This technique, known as the proper orthogonal decomposition (hereafter POD), may be applied to either experimental or numerical data to obtain a basis that captures more of the kinetic energy of the system *on average* than any other; as we shall see, the technique allows us to order the modes in terms of decreasing average energy content. We refer to these basis functions as empirical or POD modes.

The first reported instance in which POD modes were used to construct a low-dimensional model of a specific turbulent flow appeared in [3], which addressed the practically interesting problem of boundary layer turbulence. The POD was applied in the vertical, inhomogeneous direction to find optimal modes for an experimental dataset provided by Herzog [23]. The NSE, with a suitable model for the turbulent mean flow, was then projected onto the five most energetic streamwise-invariant modes. The equations were further modified to account for the energy transfer from the five retained modes to the higher order modes neglected in the truncation, thus providing a natural bifurcation parameter. The resulting equations were studied via numerical integration and analysed using dynamical systems theory. Several interesting solution regimes were identified as the bifurcation parameter was varied, including periodic, quasi-periodic, intermittent and chaotic behaviour. The most interesting of these was intermittent behaviour which, in dynamical systems terms, corresponded to a pair of heteroclinic orbits connecting two unstable fixed points. Reconstruction of the velocity field showed that the fixed points corresponded to counter-rotating rolls and the heteroclinic orbits to unstable growth, bursting, spanwise shift, and reformation of the rolls. This was interpreted as a manifestation, in the low-dimensional model, of the “burst–sweep cycle” observed in the turbulent boundary layer since [27].

The present paper is a tutorial on using the proper orthogonal decomposition to construct low-dimensional models for turbulent fluid flows. Rather than summarising the contents of the monograph [25] or review articles [9, 26], we take this opportunity to more explicitly describe key steps of the analysis, and to extend the approach. We explain two different ways to numerically calculate the POD modes (see Section 2.1) and then show how one can exploit symmetry considerations to simplify and understand such modes (see Section 2.2). By taking Fourier modes in translation-symmetric directions, one can transform a three-dimensional eigenvalue problem for the POD modes into a two-parameter family of one-dimensional problems. We show how discrete symmetries should be incorporated into the POD, and describe a specific example in considerable detail (see Section 4.1). We also comment on how parameter variations are captured naturally in ordinary differential equation (ODE) models (see Section 2.4). Finally, we describe of a generalization of the procedure for deriving ODE models, by projection onto uncoupled POD modes that allow streamwise and cross-stream components to evolve

independently, thus removing non-physical constraints imposed by very low-dimensional truncations (see Section 4.3).

The organisation of the paper is as follows. Section 2 contains a general discussion of the POD, including the rôle of symmetry, and how ODE models are obtained by Galerkin projection. In Section 3, we introduce plane Couette flow (PCF), which provides an instructive example for the application of these techniques. We focus on a minimal flow unit (MFU), where minimality refers to the spanwise and streamwise extent of the spatial domain, which are reduced (in numerical simulations) until turbulence with reasonable statistics is just sustainable. By constraining the flow to a domain that supports only one or two coherent structures, one hopes that the dynamical interactions that sustain turbulence will be sufficiently simplified that better understanding of physical mechanisms will result. In Section 4, we apply the techniques described in Section 2 to PCF. This includes detailed discussions of how the discrete symmetries of PCF can be used to simplify and understand the POD modes, and how one can uncouple the POD modes to allow streamwise and cross-stream components to evolve independently. We then summarize the behaviour of two different low-dimensional models for MFU PCF turbulence in Section 5, with one model involving coupled modes and the other uncoupled modes; this section draws heavily upon [46]. Finally, we present concluding thoughts in Section 6.

2. Finding, Understanding and Using the POD Modes

The POD procedure¹ delivers sets of empirical eigenfunctions $\{\varphi^{(n)}\}$ which approximate typical members of a data ensemble $\mathcal{U} = \{u_{(k)}\}$ better than representations of the same dimension in terms of any other bases [25]. The data ensemble, which may contain scalar- or vector-valued functions $u_{(k)}$, can be obtained experimentally, as in [3], or via numerical simulations, as in the example considered later in this paper. Specifically, we seek φ such that the quantity

$$\frac{\langle |(u, \varphi)|^2 \rangle}{\|\varphi\|^2} \tag{3}$$

is maximised. Here (\cdot, \cdot) and $\|\cdot\|$ denote an appropriate inner product and norm for the space $L^2(\Omega_x)$ of square-integrable functions, e.g.,

$$(f, g) = \int_{\Omega_x} f \cdot g^* dx \quad \text{and} \quad \|\varphi\|^2 = (\varphi, \varphi) = \int_{\Omega_x} |\varphi|^2 dx, \tag{4}$$

where Ω_x is the domain of interest over which $u_{(k)}(x)$ and $\varphi(x)$ are defined, the dot denotes a standard vector dot product, and $*$ denotes complex conjugation. In (3), $\langle \cdot \rangle$ denotes the ensemble average, but in the following we shall appeal to ergodicity to equate the ensemble average with a time average over a single solution of the NSE.

One may apply the variational calculus to recast this problem as the solution of the following Euler–Lagrange integral equation [25]:

$$\int_{\Omega_x} (u(x) \otimes u^*(x')) \varphi(x') dx' = \lambda \varphi(x), \tag{5}$$

¹ As noted in [25] the POD goes by several different names in other disciplines, including Karhunen–Loève decomposition, principal components analysis, singular systems analysis and singular value decomposition.

where \otimes is the tensor product. This is a Fredholm equation of the second kind, the kernel of which is the autocorrelation tensor averaged over the data ensemble:

$$R(x, x') \stackrel{\text{def}}{=} \langle u(x) \otimes u^*(x') \rangle. \quad (6)$$

With the norm defined as in (4) and u representing the fluid velocity, the POD modes are optimal in the sense of capturing, on average, the greatest possible fraction of total kinetic energy for a projection onto a given number of modes. Moreover the POD modes are orthogonal with respect to the inner product and can easily be made orthonormal, and each POD mode inherits linear properties from the ensemble, such as incompressibility and boundary conditions. Finally, we note that the POD procedure can be formulated for other inner products (e.g., ref. [38]), allowing the computation of POD modes which optimally represent quantities other than the kinetic energy.

2.1. DISCRETISATION OF THE EIGENVALUE PROBLEM

In practice, one solves (5) by transforming it into a matrix eigenvalue problem through suitable discretisation, then solving that problem using software such as the LAPACK numerical linear algebra package [1]. For simplicity, we consider scalar functions $u_{(k)}$ for which the tensor product in (5) is a simple product. We show here how to calculate the POD modes in two different ways: which of these requires less computational effort depends on the relative numbers of grid points, n_g , and observations or time-snapshots, N_T , in the data ensemble.

2.1.1. The Direct Method

Writing the ensemble average as a time average of the N_T snapshots and interchanging the sum and integral, we may rewrite (5) as

$$\frac{1}{N_T} \sum_{k=1}^{N_T} u_{(k)}(x) \int_{\Omega_x} u_{(k)}^*(x') \varphi(x') dx' = \lambda \varphi(x). \quad (7)$$

We may now approximate the integral over x' using either the trapezoidal rule or Simpson's rule. In both cases, we can express the integral as

$$\int_{\Omega_x} u_{(k)}^*(x) \varphi(x) dx' = \sum_{i=0}^{n_x} \omega_i u_{(k)}^*(x_i) \varphi(x_i) = \hat{\mathbf{u}}_{(k)}^* \hat{\varphi}, \quad (8)$$

where

$$\hat{\mathbf{u}}_{(k)}^* = \begin{bmatrix} \sqrt{\omega_1} u_{(k)}^*(x_1) \\ \sqrt{\omega_2} u_{(k)}^*(x_2) \\ \vdots \\ \sqrt{\omega_{n_x-1}} u_{(k)}^*(x_{n_x-1}) \\ \sqrt{\omega_{n_x}} u_{(k)}^*(x_{n_x}) \end{bmatrix}, \quad \hat{\varphi} = \begin{bmatrix} \sqrt{\omega_1} \varphi(x_1) \\ \sqrt{\omega_2} \varphi(x_2) \\ \vdots \\ \sqrt{\omega_{n_x-1}} \varphi(x_{n_x-1}) \\ \sqrt{\omega_{n_x}} \varphi(x_{n_x}) \end{bmatrix}, \quad (9)$$

and ω_i are the weight functions for the particular quadrature method used. With these definitions we may write (7) as

$$\frac{1}{N_T} \sum_{k=1}^{N_T} u_{(k)}(x) \hat{\mathbf{u}}_{(k)}^* \hat{\varphi} = \lambda \varphi(x). \quad (10)$$

In particular, this equation is satisfied at each of the n_x grid points, x_j :

$$\frac{1}{N_T} \sum_{k=1}^{N_T} u_{(k)}(x_j) \hat{\mathbf{u}}_{(k)}^* \hat{\varphi} = \lambda \varphi(x_j) \quad \text{for } j = 1, \dots, n_x. \quad (11)$$

Multiplying (11) by $\sqrt{\omega_j}$ for each $j = 1, \dots, n_x$, we may write the resulting set of equations as a single matrix-vector equation:

$$\frac{1}{N_T} \sum_{k=1}^{N_T} \hat{\mathbf{u}}_{(k)} \hat{\mathbf{u}}_{(k)}^* \hat{\varphi} \stackrel{\text{def}}{=} \tilde{\mathbf{A}} \hat{\varphi} = \lambda \hat{\varphi}. \quad (12)$$

Thus, the integral equation (5) becomes a symmetric (in general, Hermitian) eigenvalue problem for the $n_x \times n_x$ matrix $\tilde{\mathbf{A}}$. It is necessary to multiply the components of the resulting eigenvector by $1/\sqrt{\omega_j}$ to get the POD modes $\{\varphi^{(n)}\}$, but this requires very little computational effort. The modes may be normalised to ensure that they are orthonormal. Depending on whether the trapezoidal or Simpson's rule is used, the POD modes found in this way have either $\mathcal{O}(\Delta x^2)$ or $\mathcal{O}(\Delta x^4)$ error, respectively. A variant of this direct method for finding the POD modes is used, e.g., in [34, 36, 46].

2.1.2. The Method of Snapshots

It may be the case, for example for CFD databases over three-dimensional domains, that n_g , the number of grid points for each snapshot, is much larger than N_T , the total number of snapshots in our ensemble. In such situations, since we typically never require more than $\mathcal{O}(1000)$ modes, it is computationally advantageous to reformulate the computation of POD modes as an $n_T \times n_T$ eigenvalue problem, as follows. For simplicity, we again describe this only for scalar functions $u_{(k)}$, for which $n_g = n_x$.

Letting

$$c_i = \int_{\Omega_x} u_{(j)}^*(x') \varphi(x') dx',$$

Equation (7) may be rewritten as

$$\frac{1}{N_T} \sum_{j=1}^{N_T} c_j u_{(j)}(x) = \lambda \varphi(x) : \quad (13)$$

i.e. we express the eigenfunctions as linear combinations of the observations or snapshots. Multiplying both sides by $u_{(i)}^*$ and integrating yields

$$\frac{1}{N_T} \sum_{i=1}^{N_T} c_j \int_{\Omega_x} u_{(i)}^*(x) u_{(j)}(x) dx = \lambda \int_{\Omega_y} u_{(i)}^* \varphi(x) dx. \quad (14)$$

Defining

$$a_{ij} = \int_{\Omega_x} u_{(i)}^*(x) u_{(j)}(x) dx, \quad (15)$$

(14) may then be written in matrix form as

$$\begin{bmatrix} a_{11} & \cdots & a_{1N_T} \\ \vdots & & \vdots \\ a_{N_T 1} & \cdots & a_{N_T N_T} \end{bmatrix} \begin{bmatrix} c_1 \\ \vdots \\ c_{N_T} \end{bmatrix} = \lambda \begin{bmatrix} c_1 \\ \vdots \\ c_{N_T} \end{bmatrix}. \quad (16)$$

We shall denote the eigenvectors of this $N_T \times N_T$ matrix eigenvalue problem by $\mathbf{c}^n = [c_1^n \dots c_{N_T}^n]^T$ and the eigenvalues by $\lambda^{(n)}$. From (13) we see that the n th eigenfunction of the original problem can be reconstructed from the coefficients c_j^n via

$$\varphi^{(n)}(x) = \frac{1}{\lambda^{(n)} N_T} \sum_{j=1}^{N_T} c_j^n u_{(j)}(x), \quad (17)$$

or, equivalently

$$\varphi^{(n)}(x) = \frac{1}{\lambda^{(n)} N_T} [c_1^n \cdots c_{N_T}^n] \begin{bmatrix} u_{(1)}(x) \\ \vdots \\ u_{(N_T)}(x) \end{bmatrix}. \quad (18)$$

Since each ensemble member $u_{(i)}(x) = [u_{(i)}^1 \dots u_{(i)}^{n_x}]$ is specified at n_x grid points, the discretised problem (18) becomes

$$\begin{bmatrix} \varphi_1^{(1)} & \cdots & \varphi_{n_x}^{(1)} \\ \vdots & & \vdots \\ \varphi_1^{(N_T)} & \cdots & \varphi_{n_x}^{(N_T)} \end{bmatrix} = \frac{1}{N_T} \begin{bmatrix} \frac{c_1^1}{\lambda^{(1)}} & \cdots & \frac{c_{N_T}^1}{\lambda^{(1)}} \\ \vdots & & \vdots \\ \frac{c_1^{N_T}}{\lambda^{(N_T)}} & \cdots & \frac{c_{N_T}^{N_T}}{\lambda^{(N_T)}} \end{bmatrix} \begin{bmatrix} u_{(1)}^1 & \cdots & u_{(1)}^{n_x} \\ \vdots & & \vdots \\ u_{(N_T)}^1 & \cdots & u_{(N_T)}^{n_x} \end{bmatrix}. \quad (19)$$

The scalar factors are largely inconsequential since, for convenience, we normalise the eigenfunctions.

This reformulation of the original eigenvalue problem (5) is referred to as the ‘method of snapshots’ [42], and requires solution of the $N_T \times N_T$ eigenvalue problem (16) in place of the $n_x \times n_x$ problem (12). See [25] for further justification and details.

2.2. GENERAL SYMMETRY CONSIDERATIONS

Whether through their inherent geometries, modeling assumptions, or simplifying transformations such as normal forms, many solid and fluid systems have nontrivial symmetry properties. This is of interest because the presence of symmetry in a dynamical system can increase the number of critical eigenvalues at a bifurcation, imply the existence of lower dimensional invariant subspaces, and can lead

to the appearance of multiple solution branches or associated complex dynamics. Much progress in understanding the dynamics of symmetric dynamical systems has resulted from the application of the techniques of equivariant bifurcation theory [12, 14, 20, 21]. Here it is not necessary to go into the full machinery of this topic, but we do emphasise that it is important to derive ODE models which respect the appropriate symmetries of the system one wishes to study. With round-off and other discretization errors, the numerical manipulations performed in formulating and solving the eigenvalue problems above do not usually *automatically* preserve such symmetries.

Abstractly, suppose that

$$\dot{\mathbf{a}} = f(\mathbf{a}; \mu), \tag{20}$$

where $\mathbf{a} \in \mathbb{R}^n$ and $\mu \in \mathbb{R}^m$ represent dependent variables and system parameters, respectively. Let G describe a linear group acting on the dependent variables. We say that if

$$f(\gamma\mathbf{a}; \mu) = \gamma f(\mathbf{a}; \mu) \tag{21}$$

for all $\gamma \in G$, then (20) is *equivariant* with respect to the group G . This is equivalent to the statement that if $\mathbf{a}(t)$ is a solution to (20) then so is $\gamma\mathbf{a}(t)$ for all $\gamma \in G$. Indeed, acting on equation (20) with γ gives $\gamma\dot{\mathbf{a}} = \gamma f(\mathbf{a}; \mu)$. But $\gamma\dot{\mathbf{a}} = d(\gamma\mathbf{a})/dt$; also equivariance of f gives $\gamma f(\mathbf{a}; \mu) = f(\gamma\mathbf{a}; \mu)$. Thus, $d(\gamma\mathbf{a})/dt = f(\gamma\mathbf{a}; \mu)$, so $\gamma\mathbf{a}$ is also a solution.

There are two main types of symmetries: continuous and discrete. The most common type of continuous symmetry for fluid systems is translation symmetry, arising in uniform domains such as channels and pipes when periodic boundary conditions are imposed. For example, suppose that we can deduce for a physical field ψ that if $\psi(x, t)$ is a solution, then so is $\psi(x + \Delta x, t)$. Furthermore, suppose that it is reasonable to expand ψ as

$$\psi(x, t) = \mathbb{R}\{a_1(t)e^{ikx} + a_2(t)e^{2ikx} + \dots\}, \quad a_1, a_2 \in \mathbb{C};$$

here we think of the periodic boundary conditions as being imposed on a domain of length $2\pi/k$. From this ansatz, we see that the action $x \rightarrow x + \Delta x$ is equivalent to the action

$$(a_1, a_2) \mapsto (e^{ik\Delta x} a_1, e^{2ik\Delta x} a_2) \tag{22}$$

on the modal coefficients. In group theory, this is referred to as an S^1 symmetry. It is a basic result of the POD that the optimal modes in translation-invariant directions are Fourier modes [25]. Indeed, in such cases the averaged autocorrelation tensor depends only on the difference $x - x'$ and may be expanded in a Fourier series as

$$R(x - x') = \sum_k c_k e^{ik(x-x')} = \sum_k c_k e^{ikx} e^{-ikx'}, \tag{23}$$

and substituting (23) into (5), we see that $\varphi^{(k)} = e^{ikx}$ are eigenfunctions with eigenvalues c_k . Such continuous symmetries can therefore be understood in terms of an analogue of (22). This has the added bonus of reducing the dimensionality of the eigenvalue problem to be solved to find the POD modes, as described in Section 4.

The treatment of discrete symmetries in the context of the POD began with the observation in [42] that such symmetries can be used to enlarge the ensemble size without having to solve the governing

equations for new initial conditions. It was subsequently noted that, to obtain bases which appropriately retain all symmetries of the governing equations (not merely those of the data ensemble), and consequently to obtain projected ODEs with the appropriate equivariance properties, it is *necessary* to average the ensemble over the discrete symmetries [4, 10, 17, 43].

Some simple consequences follow upon calculating POD modes from ensembles which have been averaged over a discrete symmetry group G . First, if ϕ is a POD mode with eigenvalue λ , then so is $\gamma \cdot \phi$ for $\gamma \in G$. This is proved as follows. Suppose that the set of POD modes $\{\phi^{(j)}\}$ is obtained from the ensemble of snapshots $\{u_{(k)}\}$. The set of POD modes obtained from the ensemble of snapshots $\{\gamma \cdot u_{(k)}\}$ is then $\{\gamma \cdot \phi^{(j)}\}$ [17, 43]. This is true whether or not the snapshots have been averaged over the group G . However, when they *are* averaged over G , the ensembles of snapshots $\{u_{(k)}\}$ and $\{\gamma \cdot u_{(k)}\}$ are *identical*. Since they are determined by the same ensemble of snapshots, $\gamma \cdot \phi$ and ϕ are POD modes with the same eigenvalue. In fact, by linearity of the POD procedure, we have $\gamma \cdot \phi = c_\gamma \phi$ for some constant c_γ , which in general may be complex. This brief paragraph leads, in the example considered below, to the multiple pages of Section 4.1.

2.3. COMMENTS ON COMPLETENESS OF POD BASIS

The POD modes, including the (generalised) eigenfunctions with eigenvalue zero, form a complete basis for the space $L^2(\Omega_x)$. Thus, any function on Ω_x , including members of the original ensemble used to obtain them, can be represented in the L^2 sense by linear combinations of these modes. In applications, however, one is typically interested only in POD modes with strictly positive eigenvalues. (In turbulence, many things happen, but not *everything*, and we wish only to represent physically relevant events.) These no longer form a complete basis, but *almost* every member of the original ensemble can be reproduced by linear combinations of such POD modes [25]. With these considerations in mind, it is not surprising that relatively high ($\mathcal{O}(1000)$ -) dimensional projections onto POD modes can capture observed modal energy budgets and provide acceptable short-term tracking of individual solutions for turbulent flows [19, 34]. In applications, however, one often wants to consider much lower ($\mathcal{O}(10)$ -) dimensional projections, and as we shall see in the example considered in this paper, with suitable modelling of the neglected modes, very low-dimensional models are able to capture many aspects of turbulent flows. But it is important to recognise that in such low-dimensional subspaces, vector-valued eigenfunctions effectively constrain the relative magnitudes of the components of fluid velocity fields, and that this may lead to nonphysical behavior. We return to this issue in Section 4.3, where we introduce a decoupling technique to address it.

2.4. GALERKIN PROJECTION AND PARAMETER VARIATION

We obtain ODE models through Galerkin projection of the governing partial differential equations (PDEs) onto the POD modes. Abstractly, we write the evolution PDE as

$$\frac{\partial \mathbf{u}}{\partial t} = \mathbf{F}(\mathbf{u}; \mu), \quad (24)$$

where μ represents system parameters such as the Reynolds number. Expanding the function \mathbf{u} as

$$\mathbf{u}(\mathbf{x}, t) = \sum_n a_n(t) \Phi_n(\mathbf{x}),$$

and substituting this ansatz into (24), we obtain

$$\sum_n \dot{a}_n(t) \Phi_n(\mathbf{x}) = \mathbf{F} \left(\sum_n a_n(t) \Phi_n(\mathbf{x}); \mu \right).$$

Now, taking the inner product with $\Phi_m(\mathbf{x})$ and using orthonormality of the POD modes

$$\dot{a}_m(t) = \left(\mathbf{F} \left(\sum_n a_n(t) \Phi_n(\mathbf{x}); \mu \right), \Phi_m(\mathbf{x}) \right) \quad (25)$$

In the example considered below, our ensemble consists of snapshots of the flow at the same value of the Reynolds number, say Re_{ens} . However, from (25), we see that upon Galerkin projection we obtain ODEs which will explicitly contain the parameter Re . Thus, we obtain a model for the fluid flow for *all* values of Re . Of course, the POD modes are only *optimal* at Re_{ens} , so the model is expected to have the most accurate behavior for a range of Re around Re_{ens} . Although not considered for this example, it has been proposed that one can improve the range of applicability of such models by “stacking” the ensemble with snapshots over a range of parameter values; see, e.g., [44], in which this approach is applied to the Kuramoto–Sivashinsky equation.

3. Plane Couette Flow

We now describe a fluid system which serves as an instructive example for the techniques described in Section 2. In plane Couette flow (PCF), fluid is sheared between two infinite parallel plates moving at speed U_0 , in opposite directions $\pm \mathbf{e}_x$; see Figure 1. The streamwise, wall-normal, and spanwise directions are respectively x , y , and z . We non-dimensionalize lengths in units of $d/2$ where d is the gap between the plates, velocities in units of U_0 , time in units of $(d/2)/U_0$, and pressure in units of $U_0^2 \rho$ where ρ is the fluid density. Laminar flow is then given by $\mathbf{U}_0 = y \mathbf{e}_x$, $-1 \leq y \leq 1$ and the Reynolds number is $\text{Re} = \frac{U_0 d}{2\nu}$, where ν is the kinematic viscosity. Writing $\mathbf{u} = (u_1, u_2, u_3)$, $\mathbf{x} = (x, y, z)$, the evolution equation for the perturbation $(\mathbf{u}(\mathbf{x}, t), p(\mathbf{x}, t))$ to laminar flow becomes

$$\frac{\partial}{\partial t} \mathbf{u} = -(\mathbf{u} \cdot \nabla) \mathbf{u} - y \frac{\partial}{\partial x} \mathbf{u} - u_2 \mathbf{e}_x - \nabla p + \frac{1}{\text{Re}} \nabla^2 \mathbf{u}. \quad (26)$$

The fluid is assumed to be incompressible, i.e.,

$$\nabla \cdot \mathbf{u} = 0, \quad (27)$$

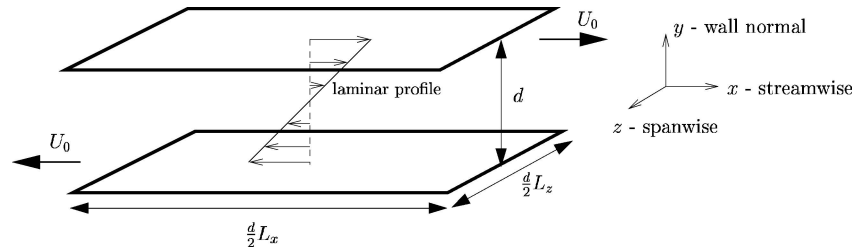


Figure 1. Geometry of plane Couette flow (PCF).

with no-slip boundary conditions at the plates, i.e.,

$$\mathbf{u}|_{y=\pm 1} = 0, \quad (28)$$

and periodicity in the streamwise and spanwise directions, with lengths $L_x = 1.75\pi$ and $L_z = 1.2\pi$, respectively. This corresponds to the MFU, the smallest domain which is able to sustain turbulence for this geometry [22]. Our POD bases or empirical eigenfunctions will be derived from a direct numerical simulation (DNS) database computed at $\text{Re} = 400$. In [34] we took the moderate aspect ratio domain $L_x = 4\pi$, $L_z = 2\pi$, also at $\text{Re} = 400$.

Equations (26)–(28) are equivariant with respect to the following symmetries [41]:

$$\mathcal{P} \cdot [(u_1, u_2, u_3, p)(x, y, z, t)] = (-u_1, -u_2, -u_3, p)(-x, -y, -z, t) \quad (29)$$

$$\mathcal{R} \cdot [(u_1, u_2, u_3, p)(x, y, z, t)] = (u_1, u_2, -u_3, p)(x, y, -z, t) \quad (30)$$

$$\mathcal{RP} \cdot [(u_1, u_2, u_3, p)(x, y, z, t)] = (-u_1, -u_2, u_3, p)(-x, -y, z, t) \quad (31)$$

$$\mathcal{T}_{\Delta x, \Delta z} \cdot [(u_1, u_2, u_3, p)(x, y, z, t)] = (u_1, u_2, u_3, p)(x + \Delta x, y, z + \Delta z, t). \quad (32)$$

Thus, if $\mathbf{u}(\mathbf{x}, t)$ solves (26), the solution obtained by acting on $\mathbf{u}(\mathbf{x}, t)$ with any product of the actions given in Equations (29)–(32) also solves it: e.g., if

$$(u_1(x, y, z, t), u_2(x, y, z, t), u_3(x, y, z, t), p(x, y, z, t))$$

solves (26), then so does

$$(u_1(x, -y, z, t), -u_2(x, -y, z, t), u_3(x, -y, z, t), p(x, -y, z, t)).$$

Physically, \mathcal{P} is a point reflection about $(x, y, z) = (0, 0, 0)$, \mathcal{R} is a reflection about the plane $z = 0$, \mathcal{RP} is a rotation by π about the z -axis, and $\mathcal{T}_{\Delta x, \Delta z}$ is a translation by Δx in the streamwise direction and by Δz in the spanwise direction. As described in [34], \mathcal{P} and \mathcal{R} generate a four element group isomorphic to the abstract group D_2 (see, e.g., ref. [32]), and altogether, with the continuous translations (32), the governing equations are equivariant with respect to the direct product $O(2) \times O(2)$. In the empirical-Fourier decomposition developed below, this corresponds to independent rotations and reflections with respect to streamwise and spanwise Fourier wavenumbers. The boundary layer model of [3] shares only *some* of these symmetries, having only $O(2) \times S^1$ symmetry (the upper wall is absent in [3], thus there is no analog of \mathcal{P} (29)). We will use (29)–(31) in our application of the POD procedure to create a basis endowed with the appropriate symmetries, and to check subsequently that the projected ODEs preserve them.

We note that PCF exhibits numerous interesting properties that a model should reproduce. Specifically, the laminar state \mathbf{U}_0 is linearly stable for all Reynolds numbers [18], but both experiments and simulations exhibit sustained turbulence for sufficiently high Re (≥ 380 – 400) and perturbation amplitudes [15, 16]. Moreover, Equation (26) possesses numerous branches of (unstable) steady states consisting of wavy streamwise vortices and streaks that arise in saddle-node bifurcations above $\text{Re} \approx 125$ [13, 37, 41], and in [41] it was suggested that turbulence might be a “chaotic repellor” formed from heteroclinic connections among such finite amplitude solutions, as in the boundary layer models of [3]. The studies in [34] support this conjecture for a moderate aspect ratio domain. For additional information, experimental work, and references on PCF, see [7, 28].

We now describe the phenomenology of MFU PCF turbulence, briefly surveying the results of [22] and presenting analogous results from our DNS; see [46] for more details. In [22] the RMS modal velocities are defined as

$$M(n_x, n_z) \stackrel{\text{def}}{=} \left(\int_{-1}^1 [\tilde{u}_1^2(n_x, y, n_z) + \tilde{u}_2^2(n_x, y, n_z) + \tilde{u}_3^2(n_x, y, n_z)] dy \right)^{1/2}, \quad (33)$$

where the tildes represent Fourier mode amplitudes, and the temporal behaviour of this quantity for various wavenumber pairs (n_x, n_z) is studied. Approximately periodic dynamics are found for certain (dominant) modal velocities; in particular, $M(0, 1)$ and $M(1, 0)$ remain in near antiphase: peaks (throughs) in the former often being accompanied troughs (peaks) in the latter: Figure 2 (cf. [22, Figure 3a]). This figure also shows that the temporal dynamics of $M(1, 1)$ is much the same as that of $M(1, 0)$, with a recurrence period is 80–100 non-dimensional time units, while $M(0, 2)$ is less regular.

Figure 3 (cf. Figure 2 in [22]) shows mid-plane contours of the streamwise velocity at the times 1–8 noted on the $M(0, 1)$ curve in Figure 2. At 1, the flow shows prominent streaks, that is, streamwise-coherent structures with variation of the streamwise velocity with respect to spanwise

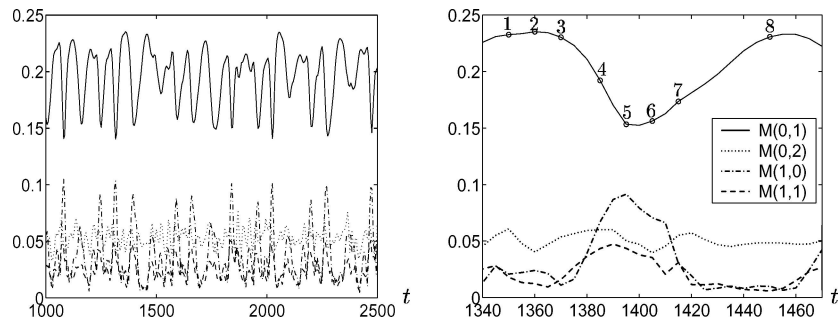


Figure 2. The behaviour of the RMS modal velocities, as defined by (33), for several wavenumber pairs: over 1500 time units of the DNS (left), and a close-up of one representative cycle (right). Here, and for similar plots throughout this paper, the legend in the right panel also applies to the left panel.

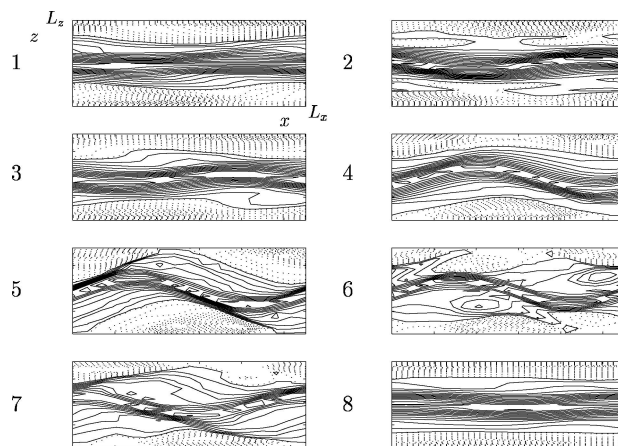


Figure 3. The streak breakdown process in DNS simulations of PCF in the MFU at eight instants in the regeneration cycle of Figure 2, as indicated by contours of u (solid positive, dashed negative) in the (x, z) plane lying between the two plates. Here, and for similar plots in this paper, we label the axes in the subplot in the upper left-hand corner only. Since the laminar solution is identically zero in this mid-plane it makes no contribution to the contours in these plots.

position. The flow pattern then develops greater variation with respect to streamwise position, until at 5 the streaks break down. They then regenerate and at 8 the process begins anew.

4. Applying POD to PCF

In fluid problems such as PCF, the snapshots $u_{(k)}$ are three-dimensional, so (5) takes the form

$$\sum_{j=1}^3 \iint \int_{\Omega_x} \langle u_i(\mathbf{x}, t) u_j^*(\mathbf{x}', t) \rangle \Phi_{jn_x n_z}^{(n)}(\mathbf{x}') d^3 \mathbf{x}' = \lambda_{n_x n_z}^{(n)} \Phi_{in_x n_z}^{(n)}(\mathbf{x}), \quad (34)$$

for $i = 1, 2, 3$, where the “quantum numbers” $n \in \mathbb{Z}^+$, and wavenumbers $n_x, n_z \in \mathbb{Z}$ distinguish different POD modes

$$\Phi_{n_x n_z}^{(n)} = (\Phi_{1n_x n_z}^{(n)}, \Phi_{2n_x n_z}^{(n)}, \Phi_{3n_x n_z}^{(n)}).$$

However, this can be recast as a family of one-dimensional eigenvalue problems to which the discretisations of Section 2.1 may be applied. As noted in Section 2.2, it is a basic result of the POD that the optimal modes in translation-invariant directions are Fourier modes [25], and we shall assume this *a priori*:

$$\Phi_{n_x n_z}^{(n)}(\mathbf{x}) = \frac{1}{\sqrt{L_x L_z}} \exp\left(2\pi i \left(\frac{n_x x}{L_x} + \frac{n_z z}{L_z}\right)\right) \phi_{n_x n_z}^{(n)}(y). \quad (35)$$

Complex conjugating (34) and using (35) implies that the complex, vector-valued “wall normal” functions $\phi_{n_x n_z}^{(n)} = (\phi_{1n_x n_z}^{(n)}, \phi_{2n_x n_z}^{(n)}, \phi_{3n_x n_z}^{(n)})$ satisfy

$$\phi_{n_x n_z}^{(n)}(y) = \phi_{-n_x, -n_z}^{(n)*}(y). \quad (36)$$

The associated expansion of the velocity field \mathbf{u} in terms of these modes is given as

$$\mathbf{u}(\mathbf{x}, t) = \sum_n \sum_{n_x} \sum_{n_z} \frac{a_{n_x n_z}^{(n)}(t)}{\sqrt{L_x L_z}} \exp\left(2\pi i \left(\frac{n_x x}{L_x} + \frac{n_z z}{L_z}\right)\right) \phi_{n_x n_z}^{(n)}(y). \quad (37)$$

and we shall refer to $\phi_{n_x n_z}^{(n)}(y)$ as the (n, n_x, n_z) POD mode. The modal coefficients $a_{n_x n_z}^{(n)}$ are complex unless $n_x = n_z = 0$. However, reality of \mathbf{u} implies that

$$a_{n_x n_z}^{(n)}(t) = a_{-n_x, -n_z}^{(n)*}(t); \quad (38)$$

hence, when we come to integrate the projected ODEs, we need compute only just over half the complex amplitudes retained in the truncation.

With this in mind, it is convenient to consider fluid flow data in the form

$$\mathbf{u}(\mathbf{x}, t) = \sum_{n_x} \sum_{n_z} \exp\left(2\pi i \left(\frac{n_x x}{L_x} + \frac{n_z z}{L_z}\right)\right) \mathbf{F}(n_x, n_z; y, t), \quad (39)$$

where reality of \mathbf{u} implies that

$$\mathbf{F}(-n_x, -n_z; y, t) = \mathbf{F}^*(n_x, n_z; y, t). \quad (40)$$

Data in this form naturally results from CFD schemes in which periodic boundary conditions are imposed and Fourier representations used in translation-invariant directions.

Substituting Equations (39) and (35) into (34), performing the integration over x' and z' , and Fourier transforming in x and z , we obtain the following family of wall-normal eigenproblems:

$$L_x L_z \sum_{j=1}^3 \int_{-1}^1 \langle F_i(n_x, n_z; y, t) F_j^*(n_x, n_z; y', t) \rangle \phi_{j, n_x, n_z}^{(n)}(y') dy' = \lambda_{n_x, n_z}^{(n)} \phi_{i, n_x, n_z}^{(n)}(y). \quad (41)$$

4.1. SYMMETRY CONSIDERATIONS: AVERAGING OVER DISCRETE SYMMETRIES

For the present system, translation symmetries in the streamwise and spanwise direction are accounted for by the Fourier decomposition (35). As discussed in Section 2.2, it is also important to average over the discrete symmetries of the system when forming the ensemble of snapshots. Suppose our original ensemble, before averaging over the symmetries, consists of T' snapshots, with $\mathbf{F}^{(k)}$ being the \mathbf{F} corresponding to the k th snapshot of \mathbf{u} . The kernel obtained by averaging over the discrete symmetry group $D_2 = \{\text{Id}, \mathcal{P}, \mathcal{R}, \mathcal{RP}\}$ is given by

$$\begin{aligned} R_{ij}(n_x, n_z; y, y') &= \langle F_i(n_x, n_z; y, t) F_j^*(n_x, n_z; y', t) \rangle \\ &= \frac{1}{T'} \sum_{l=1}^{T'} \left[\sum_{\gamma \in D_2} \gamma \cdot F_i^{(l)}(n_x, n_z; y) \gamma \cdot F_j^{(l)*}(n_x, n_z; y') \right] \\ &\stackrel{\text{def}}{=} \frac{1}{T} \sum_{k=1}^T F_i^{(k)}(n_x, n_z; y) F_j^{(k)*}(n_x, n_z; y'), \end{aligned} \quad (42)$$

where the set of snapshots is extended in the obvious way to give a total of $T = 4T'$ velocity fields. Equation (41) thus becomes

$$\frac{L_x L_z}{T} \sum_{j=1}^3 \int_{-1}^1 \sum_{k=1}^T F_i^{(k)}(n_x, n_z; y) F_j^{(k)*}(n_x, n_z; y') \phi_{j, n_x, n_z}^{(n)}(y') dy' = \lambda_{n_x, n_z}^{(n)} \phi_{i, n_x, n_z}^{(n)}(y). \quad (43)$$

Here, it may be verified from (29)–(31) and (39) that the nontrivial group elements of D_2 act on the $\mathbf{F}^{(k)}$'s as follows:

$$\mathcal{P} \cdot \begin{pmatrix} F_1^{(k)}(n_x, n_z; y) \\ F_2^{(k)}(n_x, n_z; y) \\ F_3^{(k)}(n_x, n_z; y) \end{pmatrix} = \begin{pmatrix} -F_1^{(k)}(-n_x, -n_z; -y) \\ -F_2^{(k)}(-n_x, -n_z; -y) \\ -F_3^{(k)}(-n_x, -n_z; -y) \end{pmatrix}, \quad (44)$$

$$\mathcal{R} \cdot \begin{pmatrix} F_1^{(k)}(n_x, n_z; y) \\ F_2^{(k)}(n_x, n_z; y) \\ F_3^{(k)}(n_x, n_z; y) \end{pmatrix} = \begin{pmatrix} F_1^{(k)}(n_x, -n_z; y) \\ F_2^{(k)}(n_x, -n_z; y) \\ -F_3^{(k)}(n_x, -n_z; y) \end{pmatrix}, \quad (45)$$

$$\mathcal{RP} \cdot \begin{pmatrix} F_1^{(k)}(n_x, n_z; y) \\ F_2^{(k)}(n_x, n_z; y) \\ F_3^{(k)}(n_x, n_z; y) \end{pmatrix} = \begin{pmatrix} -F_1^{(k)}(-n_x, n_z; -y) \\ -F_2^{(k)}(-n_x, n_z; -y) \\ F_3^{(k)}(-n_x, n_z; -y) \end{pmatrix}. \quad (46)$$

Although one can now discretise Equation (43) via the direct method or the method of snapshots to numerically find the POD modes, we describe a further transformation which delivers POD modes with even nicer symmetry properties. First, following the discussion in Section 2.2, we conclude that $\gamma \cdot \phi = c_\gamma \phi$ for some constant c_γ , which in general may be complex. Since $\mathcal{R}^2 = \mathcal{P}^2 = \mathcal{R}\mathcal{P}^2 = \text{Id}$, we have

$$|c_{\mathcal{R}}|^2 = |c_{\mathcal{P}}|^2 = |c_{\mathcal{R}\mathcal{P}}|^2 = 1. \quad (47)$$

Since $\mathcal{R}\mathcal{P} = \mathcal{R} \cdot \mathcal{P}$, we can also conclude that $c_{\mathcal{R}\mathcal{P}} = c_{\mathcal{R}}c_{\mathcal{P}}$. More explicitly, as shown in [34, 45], following the action of the discrete symmetries (29)–(31) through Fourier transformation and the POD, we deduce that the modal components behave as follows under the group elements:

$$\mathcal{P} \cdot \begin{pmatrix} \phi_{1,n_x,n_z}^{(n)}(y) \\ \phi_{2,n_x,n_z}^{(n)}(y) \\ \phi_{3,n_x,n_z}^{(n)}(y) \end{pmatrix} = \begin{pmatrix} -\phi_{1,-n_x,-n_z}^{(n)}(-y) \\ -\phi_{2,-n_x,-n_z}^{(n)}(-y) \\ -\phi_{3,-n_x,-n_z}^{(n)}(-y) \end{pmatrix}, \quad (48)$$

$$\mathcal{R} \cdot \begin{pmatrix} \phi_{1,n_x,n_z}^{(n)}(y) \\ \phi_{2,n_x,n_z}^{(n)}(y) \\ \phi_{3,n_x,n_z}^{(n)}(y) \end{pmatrix} = \begin{pmatrix} \phi_{1,n_x,-n_z}^{(n)}(y) \\ \phi_{2,n_x,-n_z}^{(n)}(y) \\ -\phi_{3,n_x,-n_z}^{(n)}(y) \end{pmatrix}, \quad (49)$$

$$\mathcal{R}\mathcal{P} \cdot \begin{pmatrix} \phi_{1,n_x,n_z}^{(n)}(y) \\ \phi_{2,n_x,n_z}^{(n)}(y) \\ \phi_{3,n_x,n_z}^{(n)}(y) \end{pmatrix} = \begin{pmatrix} -\phi_{1,-n_x,n_z}^{(n)}(-y) \\ -\phi_{2,-n_x,n_z}^{(n)}(-y) \\ \phi_{3,-n_x,n_z}^{(n)}(-y) \end{pmatrix}. \quad (50)$$

Consider, for example, the action of \mathcal{P} on the POD modes:

$$\begin{aligned} \mathcal{P} \cdot \phi_{n_x,n_z}^{(n)}(y) &= -\phi_{-n_x,-n_z}^{(n)}(-y) \\ &= c_{\mathcal{P}} \phi_{n_x,n_z}^{(n)}(y). \end{aligned}$$

Thus,

$$\begin{aligned} \mathcal{P}^2 \cdot \phi_{n_x,n_z}^{(n)}(y) &= \mathcal{P} \cdot [-\phi_{-n_x,-n_z}^{(n)}(-y)] \\ &= \mathcal{P} \cdot [-\phi_{n_x,n_z}^{(n)*}(-y)] \\ &= -c_{\mathcal{P}}^* \phi_{n_x,n_z}^{(n)*}(-y) \\ &= -c_{\mathcal{P}}^* \phi_{-n_x,-n_z}^{(n)}(-y) \\ &= |c_{\mathcal{P}}|^2 \phi_{n_x,n_z}^{(n)}(y). \end{aligned}$$

Since $\mathcal{P}^2 = 1$, we conclude that $|c_{\mathcal{P}}|^2 = 1$.

Now we employ the transformation

$$(\phi_{n_x,n_z}^{(n)} + \mathcal{P} \cdot \phi_{n_x,n_z}^{(n)}) / \|\phi_{n_x,n_z}^{(n)} + \mathcal{P} \cdot \phi_{n_x,n_z}^{(n)}\| \mapsto \phi_{n_x,n_z}^{(n)}, \quad (51)$$

which ensures that

$$\mathcal{P} \cdot \phi_{n_x,n_z}^{(n)} = \phi_{n_x,n_z}^{(n)}. \quad (52)$$

and, hence, $c_P = 1$, except in one special case to be described below. We note that POD modes satisfying (52) must necessarily have components of the form

$$\phi_{j,n_x,n_z}^{(k)}(y) = o(y) + ie(y) \quad (53)$$

where o and e are, respectively, odd and even functions of y . Thus POD modes lacking obvious symmetry properties will, under the transformation (51), acquire components of the form (53) and those which originally had components of the form (53) will remain unchanged. However, POD modes with components of the form

$$\phi_{j,n_x,n_z}^{(k)}(y) = e(y) + io(y). \quad (54)$$

will simply vanish altogether under the transformation (51). Each of these modes may be transformed into the form (53) by multiplying by the constant $i = \sqrt{-1}$, with the exception of the real POD modes $\phi_{j00}^{(n)}$ which, for empirical reasons, may turn out to be even in y ; for these POD modes we note that $c_P = -1$.

To investigate the action of \mathcal{R} on the POD modes, we note by explicit computation that the term which appears in the square brackets in the expression for $R_{ij}(n_x, n_z; y, y')$ in (42) is equal to

$$\begin{aligned} & \epsilon(i)\epsilon(j) [\mathcal{R} \cdot F_i^{(l)}(n_x, -n_z; y) \mathcal{R} \cdot F_j^{(l)*}(n_x, -n_z; y') \\ & + \mathcal{R} \mathcal{P} \cdot F_i^{(l)}(n_x, -n_z; y) \mathcal{R} \mathcal{P} \cdot F_j^{(l)*}(n_x, -n_z; y') \\ & + F_i^{(l)}(n_x, -n_z; y) F_j^{(l)*}(n_x, -n_z; y') \\ & + \mathcal{P} \cdot F_i^{(l)}(n_x, -n_z; y) \mathcal{P} \cdot F_j^{(l)*}(n_x, -n_z; y')] \end{aligned} \quad (55)$$

where

$$\epsilon(i) \stackrel{\text{def}}{=} \begin{cases} -1 & \text{if } i = 3 \\ 1 & \text{otherwise} \end{cases}.$$

It is thus clear that $R_{ij}(n_x, n_z; y, y') = \epsilon(i)\epsilon(j)R_{ij}(n_x, -n_z; y, y')$ or, equivalently, using $\epsilon^2 = 1$, $R_{ij}(n_x, -n_z; y, y') = \epsilon(i)\epsilon(j)R_{ij}(n_x, n_z; y, y')$. We can now see that the eigenvalue problems (43) for $\phi_{n_x,n_z}^{(n)}$ and $\phi_{n_x,-n_z}^{(n)}$ take the forms

$$\sum_{j=1}^3 \int_{-1}^1 R_{ij}(n_x, n_z; y, y') \phi_{j,n_x,n_z}^{(n)}(y') dy' = \lambda_{n_x,n_z}^{(n)} \phi_{i,n_x,n_z}^{(n)}(y) \quad (56)$$

$$\sum_{j=1}^3 \int_{-1}^1 \epsilon(i)\epsilon(j) R_{ij}(n_x, n_z; y, y') \phi_{j,n_x,-n_z}^{(n)}(y') dy' = \lambda_{n_x,-n_z}^{(n)} \phi_{i,n_x,-n_z}^{(n)}(y). \quad (57)$$

Assuming solutions $\phi_{n_x,n_z}^{(n)}(y)$ for (56), (57) is solved by taking

$$\phi_{j,n_x,-n_z}^{(n)}(y) = \epsilon(j) \phi_{j,n_x,n_z}^{(n)}(y), \quad (58)$$

with $\lambda_{n_x,-n_z}^{(n)} = \lambda_{n_x,n_z}^{(n)}$. But from (49), (58) is equivalent to saying that \mathcal{R} acts as $+1$ on the POD modes. However, note that if $n_z = 0$, (58) implies that $\phi_{3n_x,0}(y) = 0$. That is, if $n_z = 0$, our argument that \mathcal{R}

acts as +1 is only valid for modes with vanishing z -component; if the z -component does not vanish (but the other components do), we will see in the following that \mathcal{R} acts as -1 . Since $\mathcal{R}\mathcal{P} = \mathcal{R} \cdot \mathcal{P}$, where \mathcal{R} acts as ± 1 , we can also conclude that $c_{\mathcal{R}\mathcal{P}} = c_{\mathcal{R}}c_{\mathcal{P}} = \pm 1$.

We now consider the POD modes for special cases with $n_x = 0$ and/or $n_z = 0$. For simplicity of notation, we let

$$\begin{aligned} F_{aR}(y) + iF_{aI}(y) &\stackrel{\text{def}}{=} F_a^{(l)}(n_x, n_z; y), \\ G_{bR}(y') + iG_{bI}(y') &\stackrel{\text{def}}{=} F_b^{(l)}(n_x, n_z; y') \end{aligned}$$

for $a, b = 1, 2, 3$, where F_{aR} , F_{aI} , G_{bR} , and G_{bI} are real functions.

4.1.1. POD Modes with $n_x = n_z = 0$

We begin by considering the special case $n_x = n_z = 0$; the sum of these modes represents the spatially averaged flow for the system. We note that for the turbulent boundary layer system considered in [3], the mean flow was modeled as a balance between the effects of pressure and those of coherent structures; for the models considered in this paper (and in [34] and [46]), we instead calculate the mean flow with the POD procedure.

From the reality condition (40), $F_{aI}(y) = G_{bI}(y') = 0$ for $a, b = 1, 2, 3$. Then, the term in the square brackets of (42) becomes

$$\begin{aligned} &F_a^{(l)}(0, 0; y)F_b^{(l)*}(0, 0; y') + \mathcal{P} \cdot F_a^{(l)}(0, 0; y)\mathcal{P} \cdot F_b^{(l)*}(0, 0; y') + \mathcal{R} \cdot F_a^{(l)}(0, 0; y)\mathcal{R} \cdot F_b^{(l)*}(0, 0; y') \\ &\quad + \mathcal{R}\mathcal{P} \cdot F_a^{(l)}(0, 0; y)\mathcal{R}\mathcal{P} \cdot F_b^{(l)*}(0, 0; y') \\ &= (F_{aR}(y)G_{bR}(y') + F_{aR}(-y)G_{bR}(-y'))(1 + \epsilon(a)\epsilon(b)). \end{aligned} \quad (59)$$

The correlation $\langle F_a F_b^* \rangle$ in (42) thus vanishes for $(a, b) = (1, 3), (3, 1), (2, 3)$, and $(3, 2)$. Also, since there can be no mean flow in the wall normal direction, $F_{2R} = G_{2R} = 0$, so $\langle F_a F_b^* \rangle$ also vanishes for $(a, b) = (1, 2), (2, 1), (2, 2)$. The eigenvalue problem (43) therefore takes the form

$$\int_{-1}^1 R_{11}(y, y')\phi_1(y')dy' = \lambda\phi_1(y) \quad (60)$$

$$0 = \lambda\phi_2(y). \quad (61)$$

$$\int_{-1}^1 R_{33}(y, y')\phi_3(y')dy' = \lambda\phi_3(y) \quad (62)$$

where R_{11} and R_{33} are real functions. Generically, this is solved by POD modes of the form

$$\phi_{00}^{(n)}(y) = (\phi_{100}^{(n)}(y), 0, 0) \quad (63)$$

or

$$\phi_{00}^{(n)}(y) = (0, 0, \phi_{300}^{(n)}(y)). \quad (64)$$

By taking the real parts of Equations (60) and (62), we see that without loss of generality $\phi_{100}^{(n)}$ in (63) and $\phi_{300}^{(n)}$ in (64) can be taken to be real.

From (49), \mathcal{R} acts as +1 on POD modes of the form (63), and as -1 on POD modes of the form (64).

4.1.2. *POD Modes with $n_x = 0, n_z \neq 0$*

We next consider the special case of streamwise-invariant modes $n_x = 0, n_z \neq 0$. Using (40), we see that these terms in the square brackets of (42) are equal to

$$\begin{aligned}
 & F_a^{(l)}(0, n_z; y) F_b^{(l)*}(0, n_z; y') + \mathcal{P} \cdot F_a^{(l)}(0, n_z; y) \mathcal{P} \cdot F_b^{(l)*}(0, n_z; y') \\
 & \quad + \mathcal{R} \cdot F_a^{(l)}(0, n_z; y) \mathcal{R} \cdot F_b^{(l)*}(0, n_z; y') + \mathcal{R} \mathcal{P} \cdot F_a^{(l)}(0, n_z; y) \mathcal{R} \mathcal{P} \cdot F_b^{(l)*}(0, n_z; y') \\
 & = (F_{aR}(y) G_{bR}(y') + F_{aI}(y) G_{bI}(y') + F_{aR}(-y) G_{bR}(-y') \\
 & \quad + F_{aI}(-y) G_{bI}(-y')) \times (1 + \epsilon(a)\epsilon(b)) \\
 & \quad + i(F_{aI}(y) G_{bR}(y') - F_{aR}(y) G_{bI}(y') + F_{aR}(-y) G_{bI}(-y') \\
 & \quad - F_{aI}(-y) G_{bR}(-y')) \times (1 - \epsilon(a)\epsilon(b)). \tag{65}
 \end{aligned}$$

From this we can see that $R_{ab}(0, n_z; y, y')$ will be purely real if $(a, b) = (1, 1), (1, 2), (2, 1), (2, 2)$, or $(3, 3)$, and purely imaginary if $(a, b) = (1, 3), (2, 3), (3, 1)$, or $(3, 2)$. Letting $\hat{\phi}_{30n_z}^{(n)}(y) = i\phi_{30n_z}^{(n)}(y)$, the eigenvalue problem (43) takes the form

$$\int_{-1}^1 (R_{11}(y, y') \phi_1(y') + R_{12}(y, y') \phi_2(y') + R_{13}(y, y') \hat{\phi}_3(y')) dy' = \lambda \phi_1(y) \tag{66}$$

$$\int_{-1}^1 (R_{12}(y', y) \phi_1(y') + R_{22}(y, y') \phi_2(y') + R_{23}(y, y') \hat{\phi}_3(y')) dy' = \lambda \phi_2(y) \tag{67}$$

$$\int_{-1}^1 (R_{13}(y', y) \phi_1(y') + R_{23}(y', y) \phi_2(y') + R_{33}(y, y') \hat{\phi}_3(y')) dy' = \lambda \hat{\phi}_3(y), \tag{68}$$

where $R_{11}, R_{12}, R_{13}, R_{22}, R_{23}$, and R_{33} are real functions. Taking the real part of Equations (66)–(68), we conclude, without loss of generality, that ϕ_1, ϕ_2 , and $\hat{\phi}_3$ can be taken to be real or purely imaginary. That is, ϕ_1 and ϕ_2 can be taken to be real with ϕ_3 purely imaginary, or ϕ_1 and ϕ_2 can be taken to be purely imaginary with ϕ_3 real (cf. [2]). We shall make the appropriate choice to ensure that the $\phi_{0n_z}^{(n)}$ modes have components of the form (53).

Since $n_z \neq 0$, from the discussion below (58), \mathcal{R} acts as $+1$ on these POD modes. (This also follows from (49) and (36) using the properties of the modes.)

 4.1.3. *POD Modes with $n_x \neq 0, n_z = 0$*

Next, consider the special case $n_x \neq 0, n_z = 0$; such modes have no spanwise structure. Here

$$\begin{aligned}
 & F_a^{(l)}(n_x, 0; y) F_b^{(l)*}(n_x, 0; y') + \mathcal{P} \cdot F_a^{(l)}(n_x, 0; y) \mathcal{P} \cdot F_b^{(l)*}(n_x, 0; y') \\
 & \quad + \mathcal{R} \cdot F_a^{(l)}(n_x, 0; y) \mathcal{R} \cdot F_b^{(l)*}(n_x, 0; y') + \mathcal{R} \mathcal{P} \cdot F_a^{(l)}(n_x, 0; y) \mathcal{R} \mathcal{P} \cdot F_b^{(l)*}(n_x, 0; y') \\
 & = [(F_{aR}(y) G_{bR}(y') + F_{aI}(y) G_{bI}(y') + F_{aR}(-y) G_{bR}(-y') + F_{aI}(-y) G_{bI}(-y')) \\
 & \quad + i(F_{aI}(y) G_{bR}(y') - F_{aR}(y) G_{bI}(y') + F_{aR}(-y) G_{bI}(-y') \\
 & \quad - F_{aI}(-y) G_{bR}(-y'))] \times (1 + \epsilon(a)\epsilon(b)). \tag{69}
 \end{aligned}$$

From this we can see that $R_{ab}(0, n_z; y, y')$ will be nonvanishing if $(a, b) = (1, 1), (1, 2), (2, 1), (2, 2)$, or $(3, 3)$. The eigenvalue problem (43) takes the form

$$\int_{-1}^1 (R_{11}(y, y') \phi_1(y') + R_{12}(y, y') \phi_2(y')) dy' = \lambda \phi_1(y) \tag{70}$$

$$\int_{-1}^1 (R_{12}^*(y, y')\phi_1(y') + R_{22}(y, y')\phi_2(y')) dy' = \lambda\phi_2(y), \quad (71)$$

$$\int_{-1}^1 R_{33}(y, y')\phi_3(y') dy' = \lambda\phi_3(y) \quad (72)$$

where R_{11} , R_{12} , R_{22} , and R_{33} are *complex* functions. Generically, we expect POD modes of the form

$$\phi_{n_x 0}^{(n)} = (\phi_{1n_x 0}^{(n)}, \phi_{2n_x 0}^{(n)}, 0) \quad (73)$$

or

$$\phi_{n_x 0}^{(n)} = (0, 0, \phi_{3n_x 0}^{(n)}); \quad (74)$$

these POD modes are complex. We employ the transformation (51) to ensure that these modes are of the form (53).

From (49), \mathcal{R} acts as $+1$ on POD modes of the form (73), and as -1 on POD modes of the form (74).

4.1.4. *POD Modes with $n_x \neq 0$, $n_z \neq 0$*

The eigenvalue problem (43) for $n_x \neq 0$, $n_z \neq 0$ lacks the special properties of the cases considered above, and we can only conclude that \mathcal{R} acts as $+1$. Again we employ the transformation (51) to ensure that the modes are of the form (53).

4.1.5. *Summary of Group Actions on the POD Modes*

We summarise the actions of \mathcal{P} , \mathcal{R} and \mathcal{RP} on the POD modes as follows:

$$\mathcal{P} \cdot \phi_{n_x, n_z}^{(n)} = c_{\mathcal{P}} \phi_{n_x, n_z}^{(n)}, \quad (75)$$

$$\mathcal{R} \cdot \phi_{n_x, n_z}^{(n)} = c_{\mathcal{R}} \phi_{n_x, -n_z}^{(n)}, \quad (76)$$

$$\mathcal{RP} \cdot \phi_{n_x, n_z}^{(n)} = c_{\mathcal{P}} c_{\mathcal{R}} \phi_{-n_x, n_z}^{(n)}, \quad (77)$$

where

$$c_{\mathcal{P}} = \begin{cases} -1 & \text{if } n_x = n_z = 0 \text{ and } \phi_{0,0}^{(n)} \text{ has components even in } y \\ +1 & \text{otherwise} \end{cases}, \quad (78)$$

$$c_{\mathcal{R}} = \begin{cases} -1 & \text{if } n_x = n_z = 0 \text{ and } \phi_{3,0,0}^{(n)} = 0 \\ -1 & \text{if } n_z = 0 \text{ and } \phi_{1,n_x,0}^{(n)} = \phi_{2,n_x,0}^{(n)} = 0 \\ +1 & \text{otherwise} \end{cases}. \quad (79)$$

4.2. RESULTS FROM THE POD

After allowing transients to decay and a statistically stationary (turbulent) state to become established at $Re = 400$, we ran our DNS for 20,000 non-dimensional time units, assembling a database of 4000 velocity field snapshots $\{\mathbf{u}(\mathbf{x}, t_j)\}$ by recording every 500th timestep ($\Delta t = 0.01$). This ensemble was then expanded four-fold by averaging over the discrete symmetries as described above.

Table 1. Eigenvalues for the POD modes for PCF in the MFU.

| (n, n_x, n_z) | $\lambda_{n_x, n_z}^{(n)}$ | $\% E_{n_x, n_z}^{(n)}$ |
|-------------------------|----------------------------|-------------------------|
| (1, 0, 0) | 4.4550 | 68.02 |
| (1, 0, ± 1) | 0.7821 | 23.88 |
| (1, 0, ± 2) | 0.0543 | 1.66 |
| (1, ± 1 , 0) | 0.0386 | 1.18 |
| (1, 0, ± 3) | 0.0195 | 0.59 |
| (2, 0, 0) | 0.0174 | 0.27 |
| (2, 0, ± 1) | 0.0123 | 0.38 |
| (1, ± 1 , ± 2) | 0.0109 | 0.33 |
| (1, ± 1 , ± 1) | 0.0090 | 0.27 |
| (3, 0, 0) | 0.0068 | 0.10 |
| (4, 0, 0) | 0.0054 | 0.08 |
| (3, 0, ± 1) | 0.0039 | 0.12 |
| ... | | |

Table 1 lists the eigenvalues associated with the first twelve (sets of) POD modes in order of decreasing eigenvalue magnitude. Here

$$\% E_{n_x, n_z}^{(n)} \stackrel{\text{def}}{=} \left(\lambda_{n_x, n_z}^{(n)} / \sum_{m, m_x, m_z} \lambda_{m_x, m_z}^{(m)} \right) \times 100$$

is the percentage of average total energy contained in the (n, n_x, n_z) POD mode. The symmetries guarantee that $\lambda_{n_x, n_z}^{(n)} = \lambda_{n_x, -n_z}^{(n)}$, and we lump these modes together accordingly.

The three most energetic modes have Fourier wavenumbers (0, 0), (0, 1), (0, 2); a similar triad appeared in the Moderate Aspect Ratio PCF study of [34]. Interestingly, the fourth most energetic mode is the spanwise-invariant (1, 1, 0) mode, which has neither a streamwise nor a wall-normal component and is thus unable to directly interact with the (1, 0, 0) mode representing the mean flow. In Figure 4 we show the (1, 0, 0) mode and indicate its close approximation to the full (DNS) mean velocity profile. The next four “two-dimensional modes” that follow the (1, 0, 0) mode in Table 1 are plotted in Figure 5. Over 90% of the turbulent kinetic energy is captured by the first two modes, while 99% is captured by the leading 43 modes. Table 1 agrees well with independent results of [19].

See Figures 6–9 for a verification of some of the symmetry properties of the POD modes discussed in Section 4.1.

4.3. UNCOUPLED POD MODES

Commenting on the wall layer model of [3] which uses only streamwise-invariant modes ($n_x = 0$ in the present notation) presented in [24], Moffatt [35] pointed out that, based on fundamental considerations, all disturbances should eventually decay unless streamwise variations are included. Indeed, for streamwise-invariant flow, for which the convective derivative reduces to

$$D/Dt = \partial/\partial t + u_2 \partial/\partial y + u_3 \partial/\partial z, \tag{80}$$

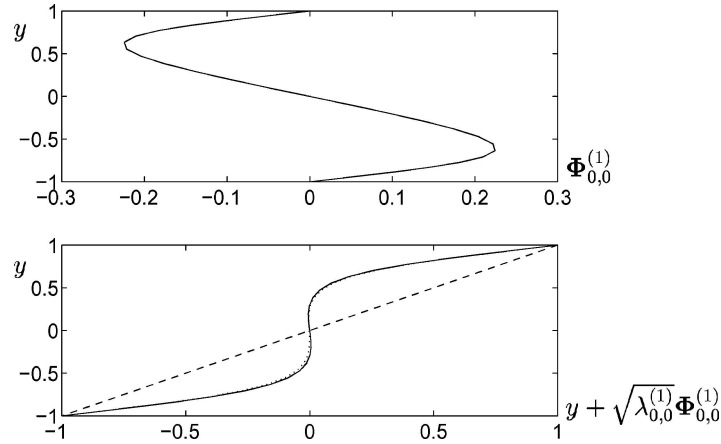


Figure 4. The x -component of the POD mode $\Phi_{0,0}^{(1)}$ (top). The y and z -components are equal to zero. The velocity profile obtained by adding this POD mode with r.m.s. amplitude $\sqrt{\lambda_{0,0}^{(1)}} = \sqrt{(|a_{0,0}^{(1)}(t)|^2)}$ to the laminar state $\mathbf{U}_0 = z\mathbf{e}_x$ (bottom). The mean flow obtained from the full DNS ensemble average is also indicated (dotted curve, barely discernible).

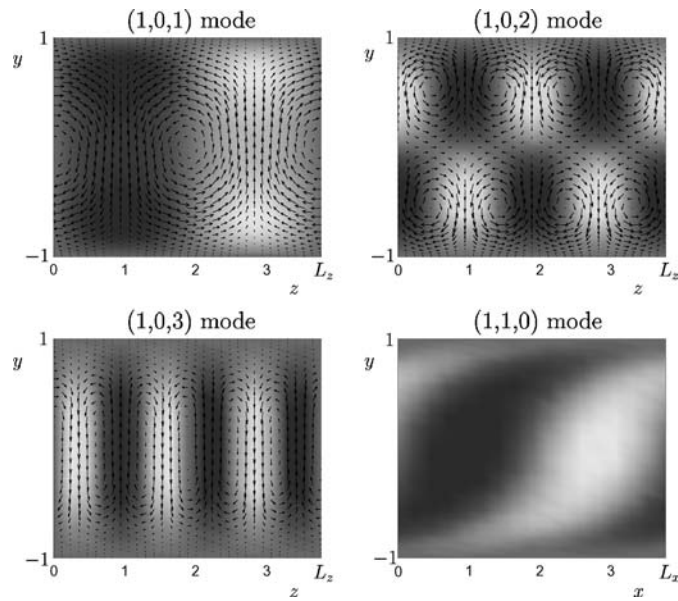


Figure 5. Flow fields \mathbf{u} associated with the $(n, n_x, n_z) = (1, 0, 1)$, $(1, 0, 2)$, $(1, 0, 3)$ and $(1, 1, 0)$ POD modes. For the $(1, 0, 1)$, $(1, 0, 2)$ and $(1, 0, 3)$ POD modes the vectors show the spanwise and wall-normal velocities, while the dark (light) shading denotes positive (negative) streamwise velocity. For the $(1, 1, 0)$ mode the u and v components are identically zero, and the dark (light) shading now denotes positive (negative) spanwise velocity.

the x -component of the Navier–Stokes equation is

$$\frac{D}{Dt}(U + u_1) = \frac{1}{\text{Re}} \left(\frac{\partial^2}{\partial y^2} + \frac{\partial^2}{\partial z^2} \right) (U + u_1), \quad (81)$$

where U denotes the laminar profile, entirely in the x -direction, and $u_{1,2,3}$ are the fluctuations. (Note that u_2 and u_3 influence the dynamics of u_1 , but u_1 does not influence the dynamics of u_2 and u_3 .)

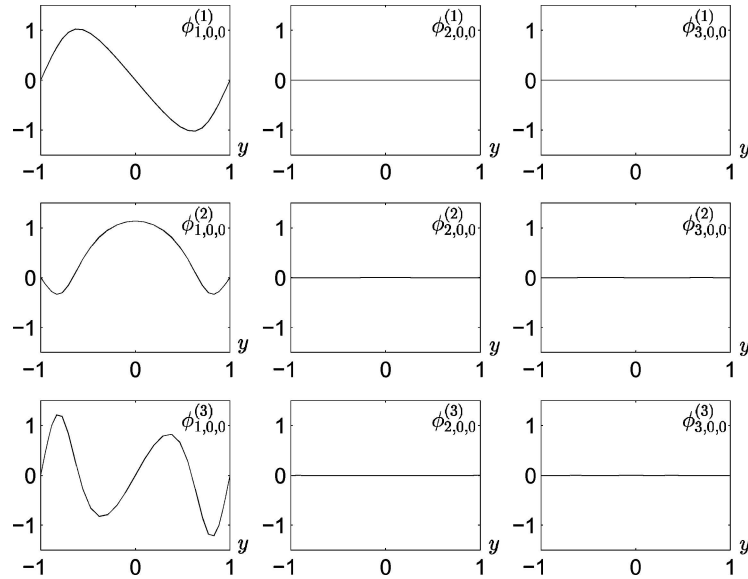


Figure 6. The three most energetic (real) POD modes for the $(n_x, n_z) = (0, 0)$ Fourier pair. All modes have zero component in the y and z directions; the x component of the $n = 1, 3$ modes are odd, whilst that for the $n = 2$ mode is even.

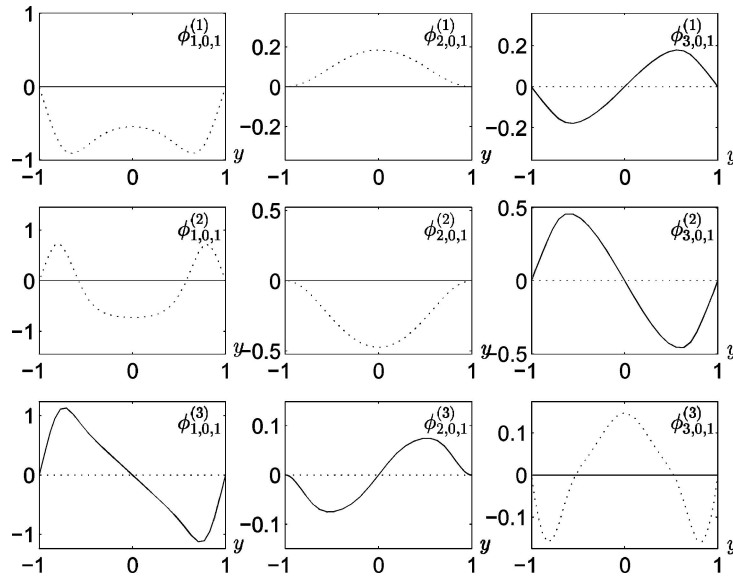


Figure 7. The three most energetic POD modes for the $(n_x, n_z) = (0, 1)$ Fourier pair, with real and imaginary parts indicated by solid and dashed lines, respectively.

Furthermore, it can be shown that

$$\frac{d}{dt} \iint (u_2^2 + u_3^2) dy dz = -2\nu \left\{ \iint \omega_x^2 dy dz \right\}, \tag{82}$$

where ω_x is the x -component of the vorticity, showing that the energy in the cross-stream components of the velocity must decay to zero. In the long-time limit then, in (81), $D/Dt \rightarrow \partial/\partial t$, giving a simple diffusion equation for u_1 . Hence at large time u_1 tends to a constant value, the only possible

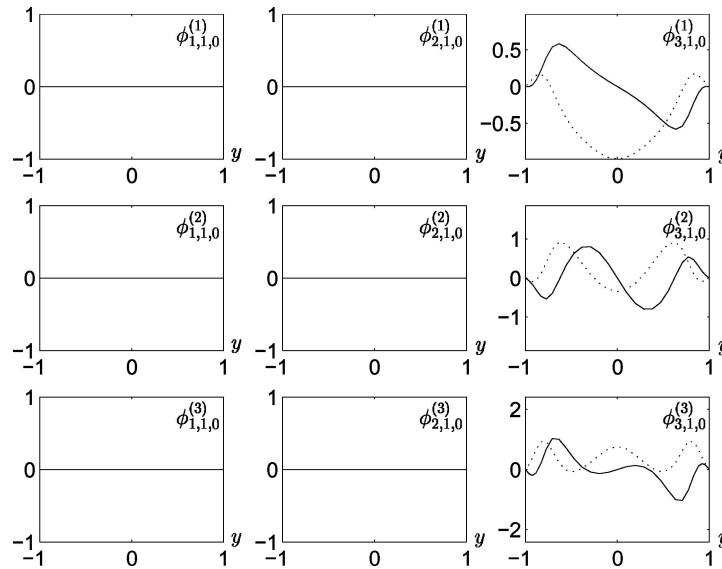


Figure 8. The three most energetic POD modes for the $(n_x, n_z) = (1, 0)$ Fourier pair, with real and imaginary parts indicated by solid and dashed lines, respectively.

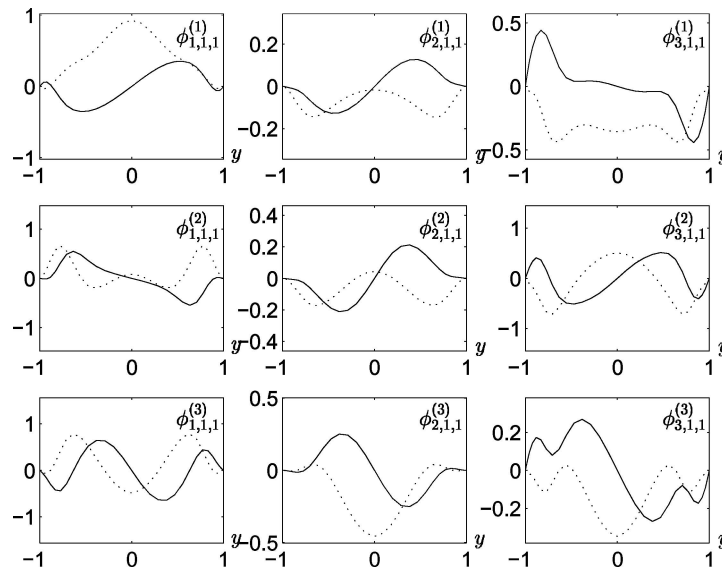


Figure 9. The three most energetic POD modes for the $(n_x, n_z) = (1, 1)$ Fourier pair, with real and imaginary parts indicated by solid and dashed lines, respectively.

solution being $u_1 = 0$, and although the streamwise velocity may experience transient growth due the cross-stream flow, it must also eventually vanish.

As pointed out in an addendum to [24] and in more detail in [8], each vector-valued POD eigenfunction determines the relative magnitudes of streamwise and cross-stream components in that mode. In particular, this implies that the inner product in the second term in the linear coefficients $\hat{A}_{n_x, n_z}^{(n, k)}$ of Equation (93), below, is strictly positive for $n_x = 0$. This term provides the energy source. The constraint imposed by projection onto streamwise-invariant modes that (correctly) represent the typical

behaviour with streamwise variations present, imposes coupling that can maintain streamwise velocity fluctuations. Completeness of the POD basis implies that, if sufficiently many empirical eigenfunctions are included, linear combinations exist that effectively decouple streamwise and cross-stream components and restore the appropriate, eventually-decaying behaviour. However, to remove the coupling constraint in the (very) low-dimensional truncations of interest here, we must allow the streamwise and cross-stream velocity components of streamwise invariant modes to evolve separately.

Following the suggestion of Waleffe [48], we construct a pair of “uncoupled” basis functions from each empirical eigenfunction by decomposing it into mutually orthogonal components:

$$\Phi_{n_x, n_z}^{(n)}(\mathbf{x}) = \Phi_{n_x, n_z}^{(n)[1]}(\mathbf{x}) + \Phi_{n_x, n_z}^{(n)[2]}(\mathbf{x}), \quad (83)$$

where

$$\Phi_{n_x, n_z}^{(n)[1]}(\mathbf{x}) \stackrel{\text{def}}{=} P_{n_x, n_z} \Phi_{n_x, n_z}^{(n)}(\mathbf{x}), \quad \Phi_{n_x, n_z}^{(n)[2]}(\mathbf{x}) \stackrel{\text{def}}{=} (I - P_{n_x, n_z}) \Phi_{n_x, n_z}^{(n)}(\mathbf{x}) \quad (84)$$

and the projection matrix is defined by

$$P_{n_x, n_z} \stackrel{\text{def}}{=} pp^T / (p^T p) \quad \text{with} \quad p \stackrel{\text{def}}{=} [-2\pi n_z / L_z, 0, 2\pi n_x / L_x]^T. \quad (85)$$

Here $\Phi_{n_x, n_z}^{(n)[1]}(\mathbf{x})$ and $\Phi_{n_x, n_z}^{(n)[2]}(\mathbf{x})$ are of the form (35) with

$$\phi_{n_x, n_z}^{(n)[1]}(y) = \begin{pmatrix} a\phi_{1, n_x, n_z}^{(n)}(y) - b\phi_{3, n_x, n_z}^{(n)}(y) \\ 0 \\ -b\phi_{1, n_x, n_z}^{(n)}(y) + c\phi_{3, n_x, n_z}^{(n)}(y) \end{pmatrix}, \quad (86)$$

and

$$\phi_{n_x, n_z}^{(n)[2]}(y) = \begin{pmatrix} (1 - a)\phi_{1, n_x, n_z}^{(n)}(y) + b\phi_{3, n_x, n_z}^{(n)}(y) \\ \phi_{2, n_x, n_z}^{(n)}(y) \\ b\phi_{1, n_x, n_z}^{(n)}(y) + (1 - c)\phi_{3, n_x, n_z}^{(n)}(y) \end{pmatrix}, \quad (87)$$

respectively, appearing in the place of $\phi_{n_x, n_z}^{(n)}(y)$, and where

$$a \stackrel{\text{def}}{=} \frac{n_z^2 / L_z^2}{n_x^2 / L_x^2 + n_z^2 / L_z^2}, \quad b \stackrel{\text{def}}{=} \frac{n_x n_z / (L_x L_z)}{n_x^2 / L_x^2 + n_z^2 / L_z^2}, \quad c \stackrel{\text{def}}{=} \frac{n_x^2 / L_x^2}{n_x^2 / L_x^2 + n_z^2 / L_z^2}.$$

The streamwise- and spanwise-invariant modes therefore take the forms

$$\phi_{0, n_z}^{(n)[1]}(y) = \begin{pmatrix} \phi_{1, 0, n_z}^{(n)}(y) \\ 0 \\ 0 \end{pmatrix}, \quad \phi_{0, n_z}^{(n)[2]}(y) = \begin{pmatrix} 0 \\ \phi_{2, 0, n_z}^{(n)}(y) \\ \phi_{3, 0, n_z}^{(n)}(y) \end{pmatrix}, \quad (88)$$

$$\phi_{n_x, 0}^{(n)[1]}(y) = \begin{pmatrix} 0 \\ 0 \\ \phi_{3, n_x, 0}^{(n)}(y) \end{pmatrix}, \quad \phi_{n_x, 0}^{(n)[2]}(y) = \begin{pmatrix} \phi_{1, n_x, 0}^{(n)}(y) \\ \phi_{2, n_x, 0}^{(n)}(y) \\ 0 \end{pmatrix}, \quad (89)$$

and for modes with neither streamwise nor spanwise variation we have $\phi_{0,0}^{(n)[1]}(y) = 0$, $\phi_{0,0}^{(n)[2]}(y) = \phi_{0,0}^{(n)}(y)$. We also note that the functions are pairwise-orthogonal and divergence-free:

$$(\Phi_{n_x, n_z}^{(n)[m]}(\mathbf{x}), \Phi_{n_x, n_z}^{(n')[m']}(\mathbf{x})) = e_{n_x, n_z}^{(n)[m]} \delta_{nn'} \delta_{mm'}, \quad (90)$$

$$\nabla \cdot \Phi_{n_x, n_z}^{(n)[m]}(\mathbf{x}) = 0 \quad \text{for } m = 1, 2. \quad (91)$$

We do not normalise the uncoupled modes, hence the (non-unity) coefficients $e_{n_x, n_z}^{(n)[m]}$; however, we have $e_{n_x, n_z}^{(n)[1]} + e_{n_x, n_z}^{(n)[2]} = 1$.

For $n_x = 0$ we recover the decomposition of [8], but in general neither term in the decomposition represents a purely streamwise or cross-stream component. For $n_x, n_z \neq 0$, $\phi_{n_x, n_z}^{[1]}(y)$ represents a structure that lies parallel with the walls at $y = \pm 1$, while $\phi_{n_x, n_z}^{[2]}(y)$ is fully three-dimensional, cf. (86)–(87).

5. Low-Dimensional MFU PCF Models

In this section we derive and describe the behaviour of two low-dimensional models for PCF, one involving the coupled empirical eigenfunctions provided by the POD procedure, and the other using the decoupled basis of Section 4.3.

5.1. LOW-DIMENSIONAL MODELS FOR THE MFU USING COUPLED MODES

5.1.1. Structure of the Equations

We first briefly describe the general derivation and some properties of the ODEs resulting from Galerkin projection of the Navier–Stokes equations onto subspaces spanned by sets of POD modes, as sketched in Section 2.4. Inserting (37) into (26) and performing a Galerkin projection, we obtain ODEs of the form

$$\dot{a}_{n_x, n_z}^{(n)} = \sum_{k=1}^{\infty} \hat{A}_{n_x, n_z}^{(n,k)} a_{n_x, n_z}^{(k)} + [N(\mathbf{a}, \mathbf{a})]_{n_x, n_z}, \quad (92)$$

$$n = 1, 2, \dots, \quad n_x, n_z = \dots, -2, -1, 0, 1, 2, \dots,$$

where

$$[N(\mathbf{a}, \mathbf{a})]_{n_x, n_z} \stackrel{\text{def}}{=} \sum_{\substack{m, k, \\ m_x, m_z}} \hat{B}_{n_x, n_z, m_x, m_z}^{(n, m, k)} a_{m_x, m_z}^{(m)} a_{n_x - m_x, n_z - m_z}^{(k)}.$$

The reality condition (38) implies that we may exclude about half these equations: if $n_x = 0$ (resp. $n_z = 0$) it suffices to consider only $n_z \geq 0$ (resp. $n_x \geq 0$), and if $n_x, n_z \neq 0$ we may still take only $n_x \geq 0$ (or $n_z \geq 0$).

Letting ' denote differentiation with respect to y , the coefficients in (92) are:

$$\begin{aligned} \hat{A}_{n_x, n_z}^{(n,k)} &\stackrel{\text{def}}{=} -\frac{1}{\text{Re}} \left(\left(\frac{2\pi n_x}{L_x} \right)^2 + \left(\frac{2\pi n_z}{L_z} \right)^2 \right) \delta_{nk} \\ &\quad - \int_{-1}^1 \phi_{2, n_x, n_z}^{(n)} \phi_{1, n_x, n_z}^{(k)*} dy - \frac{2\pi i n_x}{L_x} \sum_{j=1}^3 \int_{-1}^1 y \phi_{j, n_x, n_z}^{(n)} \phi_{j, n_x, n_z}^{(k)*} dy \\ &\quad - \frac{1}{\text{Re}} \sum_{j=1}^3 \int_{-1}^1 \phi_{j, n_x, n_z}^{(n)'} \phi_{j, n_x, n_z}^{(k)*'} dy, \end{aligned} \quad (93)$$

$$\begin{aligned} \hat{B}_{n_x, n_z, m_x, m_z}^{(n, m, k)} \stackrel{\text{def}}{=} & -\frac{1}{\sqrt{L_x L_z}} \sum_{j=1}^3 \int_{-1}^1 \left(\frac{2\pi i m_x}{L_x} \phi_{1, n_x - m_x, n_z - m_z}^{(k)} \phi_{j m_x m_z}^{(m)} \right. \\ & \left. + \phi_{2, n_x - m_x, n_z - m_z}^{(k)} \phi_{j m_x m_z}^{(m)'} + \frac{2\pi i m_z}{L_z} \phi_{3, n_x - m_x, n_z - m_z}^{(k)} \phi_{j m_x m_z}^{(m)} \right) \phi_{j, n_x, n_z}^{(n)*} dy. \end{aligned} \quad (94)$$

The projected ODEs (92) are equivariant (see Section 2.2) with respect to the continuous symmetries

$$\mathcal{T}_{\Delta x} : a_{n_x, n_z}^{(n)}(t) \mapsto e^{i n_x \phi_x} a_{n_x, n_z}^{(n)}(t), \quad (95)$$

$$\mathcal{T}_{\Delta z} : a_{n_x, n_z}^{(n)}(t) \mapsto e^{i n_z \phi_z} a_{n_x, n_z}^{(n)}(t), \quad (96)$$

where $\phi_x = 2\pi \Delta x / L_x$ and $\phi_z = 2\pi \Delta z / L_z$. Furthermore, from the symmetries of the POD modes described in Section 4.1, the equations must also be equivariant with respect to the following discrete actions of \mathcal{P} , \mathcal{R} , and \mathcal{RP} on the modal amplitude coefficients $a_{n_x, n_z}^{(n)}$:

$$\mathcal{P} \cdot a_{n_x, n_z}^{(n)}(t) = c_{\mathcal{P}} a_{-n_x, -n_z}^{(n)}(t), \quad (97)$$

$$\mathcal{R} \cdot a_{n_x, n_z}^{(n)}(t) = c_{\mathcal{R}} a_{n_x, -n_z}^{(n)}(t), \quad (98)$$

$$\mathcal{RP} \cdot a_{n_x, n_z}^{(n)}(t) = c_{\mathcal{P}} c_{\mathcal{R}} a_{-n_x, n_z}^{(n)}(t), \quad (99)$$

where the coefficients $c_{\mathcal{P}}$ and $c_{\mathcal{R}}$ are given in (78) and (79), respectively.

This implies that many terms which might ostensibly appear in (92) are, in fact, absent. Also, by exploiting symmetry properties of the POD modes (specifically, oddness or evenness of components $\phi_{i, n_x, n_z}^{(n)}$ under $y \rightarrow -y$), it can be shown that others among the \hat{A} and \hat{B} coefficients vanish identically. Finally, the nonlinear terms in the Navier–Stokes equations are energy-conserving. Specifically, we have

$$\begin{aligned} & \int \int \int_{\Omega_x} \mathbf{u} \cdot (\mathbf{u} \cdot \nabla \mathbf{u}) d^3 \mathbf{x} \\ &= \int \int \int_{\Omega_x} \mathbf{u} \cdot \left(\nabla \left(\frac{1}{2} \mathbf{u} \cdot \mathbf{u} \right) - \mathbf{u} \times (\nabla \times \mathbf{u}) \right) d^3 \mathbf{x} \\ &= \int \int \int_{\Omega_x} \nabla \cdot \left(\left(\frac{1}{2} \mathbf{u} \cdot \mathbf{u} \right) \mathbf{u} \right) d^3 \mathbf{x} \\ &= \int \int_{\partial \Omega_x} \left(\frac{1}{2} \mathbf{u} \cdot \mathbf{u} \right) \mathbf{u} \cdot \hat{\mathbf{n}} dS = 0, \end{aligned} \quad (100)$$

where we have used vector identities, the facts that $\mathbf{u} \cdot (\mathbf{u} \times (\nabla \times \mathbf{u})) = 0$ and $\nabla \cdot \mathbf{u} = 0$, and the divergence theorem. The surface integral vanishes due to the no-slip boundary conditions at $z = \pm 1$ and periodicity in the x and z -directions. Using (37), it can be shown that Equation (100) is equivalent to

$$\sum_{n_x=-\infty}^{\infty} \sum_{n_z=-\infty}^{\infty} \sum_{n_z=-\infty}^{\infty} a_{n_x, n_z}^{(n)*} [N(\mathbf{a}, \mathbf{a})]_{n, n_x, n_z} = 0. \quad (101)$$

Equation (101) and the symmetries (95)–(99) provide checks on the numerically computed nonlinear coefficients: in all cases for MFU PCF turbulence at $\text{Re} = 400$ we found that (101) is satisfied to

0.01%, and we subsequently rounded off the coefficients to ensure that these symmetries are exactly respected.

The ODEs (92) are similar to those of the turbulent boundary layer problem in [3], with the following important differences. In [3], in place of $\mathbf{U}_0 = \mathbf{y}e_x$, the analog of (26) involves a spatially-averaged (t -dependent) mean turbulent velocity, modeled as a balance between the effects of pressure and those of the coherent structures, giving cubic terms in the ODEs. No such modeling is required here: the nonlinear terms derive directly from (26) and the $n_x = n_z = 0$ modes represent time-varying turbulent modifications to the mean. Second, the contribution from the pressure term at the outer edge of the wall layer was modeled as stochastic forcing in [3]; here, it makes no contribution because of the divergence-free expansion (37) and no-slip and periodic conditions at the boundaries of Ω_x [25]. Finally, in [3] the ODEs are equivariant under $O(2) \times S^1$; here, the additional reflection \mathcal{R} and rotation \mathcal{RP} symmetries make the ODEs equivariant under $O(2) \times O(2)$, further constraining the modal interactions.

5.1.2. Behaviour of a Six Coupled-Mode Model

In [46], it is argued that a good model for turbulent MFU PCF is obtained by projection onto the six modes $(n, n_x, n_z) = (1, 0, 0), (1, 0, 1), (1, 0, 2), (1, 1, 0)$ and $(1, 1, \pm 1)$. Referring to Table 1, we see that these are *not* simply the six most energetic modes, but rather the top four and the tenth and eleventh. In general, it was found that obtaining low-dimensional models which capture the desired dynamics required careful consideration of how the modes interact with each other, along with a modest amount of trial and error. Here $(1, 1, \pm 1)$ is included since it is fully three-dimensional and couples relatively strongly with the $(1, 0, 1), (1, 0, 2)$ and $(1, 1, 0)$ modes. See [46] for explicit statements of the ODEs.

Throughout this section all computations are done at $\text{Re} = 400$, as for the DNS data used to compute the POD basis. Integration of this 11-dimensional dynamical system ($a_{0,0}^{(1)}$ is real, all other amplitudes are complex), without modelling losses to neglected modes, reveals travelling waves of the form

$$a_{n_x, n_z}^{(n)} = r_{n_x, n_z}^{(n)} \exp(i(-\omega n_z t + \alpha_{n_x, n_z}^{(n)})), \quad (102)$$

where the reality of $a_{0,0}^{(1)}$ requires that $\alpha_{0,0}^{(1)}$ is necessarily zero. The amplitudes of the $(1, 0, 0), (1, 0, 1)$ and $(1, 0, 2)$ modes are plotted in Figure 10 in comparison with the “true” modal amplitudes obtained by projecting the DNS onto these modes, denoted $\hat{a}_{0,j}$. Note that $\hat{a}_{0,1}^{(1)}$ and $\hat{a}_{0,2}^{(1)}$ are approximately confined to a “thickened” torus: each oscillating relatively quickly along a radius and drifting more slowly and chaotically around the circumference. The model fails to reproduce the radial motion, and caricatures

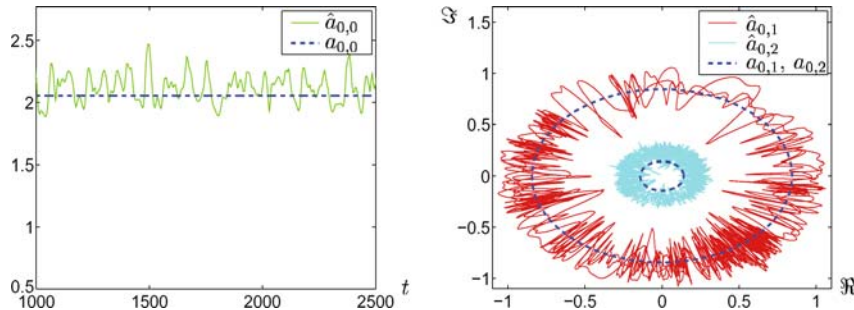


Figure 10. Behaviour of the six coupled-mode model compared to the DNS projected onto the $(1, 0, 0), (1, 0, 1)$ and $(1, 0, 2)$ modes. Here each of $a_{0,0}, a_{0,1}, a_{0,2}$ are shown as dashed lines, and are intended to represent approximations to the nearest (noisy) \hat{a}_{n_x, n_z} line. The superscript (1) has been dropped from the labels for clarity.

the circumferential motion as a simple travelling wave with a relatively low period of 65.9 time units. It is clear from Figure 10 that the average of the projected (1, 0, 0), (1, 0, 1) and (1, 0, 2) modal amplitudes is well-approximated by the travelling wave model.

The travelling wave solution is, however, entirely unsatisfactory from a dynamical viewpoint. The RMS modal velocities, calculated from

$$M(n_x, n_z) = \frac{1}{\sqrt{L_x L_z}} \sum_n |a_{n_x, n_z}^{(n)}|^2, \quad (103)$$

are constant, since the modal amplitudes are constant; hence the regeneration cycle identified in [22] (Figures 2 and 3 above) is completely absent. Substituting (102) into the Galerkin approximation (37) shows that the travelling waves (102) represent streak/vortex structures moving in the spanwise direction at speed $\omega L_z / (2\pi)$.

In [46], we model the losses to the neglected modes by adding terms of the form

$$-\alpha \nu (n_x^2 + n_z^2) a_{n_x, n_z}^{(n)},$$

to the equations for $\dot{a}_{n_x, n_z}^{(n)}$. Through suitable averaging (see [46]), we found that $\nu = 0.0333$. We then adjusted the $\mathcal{O}(1)$ parameter α to obtain the best fit between the behaviour of the model and the DNS. A representation analogous to Figure 10 for $\alpha = 0.8$ appears as Figure 11. The traveling waves of Figure 10 are replaced by standing waves that appear as radial segments in the projections of Figure 11. As we shall see, these capture the regeneration cycle fairly well, with appropriate amplitudes for the complex modes (1, 0, 1) and (1, 0, 2), although the amplitude of the (1, 0, 0) “mean flow” mode in the model is significantly lower than in the projected DNS (Figure 11, left panel).

The RMS modal velocities for the model, calculated from (103), are presented in the right panel of Figure 12, for comparison with analogous DNS quantities, re-plotted in the left panel (cf. Figure 2). Here, and for similar plots in this paper, we present in the left panel the analogous quantities for the DNS with only those modes present in the low-dimensional model included in the projection, i.e. (103) with $a_{n_x, n_z}^{(n)}$ replaced by $\hat{a}_{n_x, n_z}^{(n)}$. In neither case do we sum over n , since only one quantum number is included in the models considered in this paper. The cyclic behaviour is essentially reproduced: $M(0, 1)$ and $M(1, 0)$ are approximately of opposite phase, while the latter is approximately in phase with $M(1, 1)$. The magnitudes of the RMS modal velocities also compare well with those from the DNS.

In Figure 13 we show reconstructed model velocity fields at the time instants 1'–8' marked on the right panel of Figure 12 (analogous to 1–8 on the left), for comparison with analogous quantities from

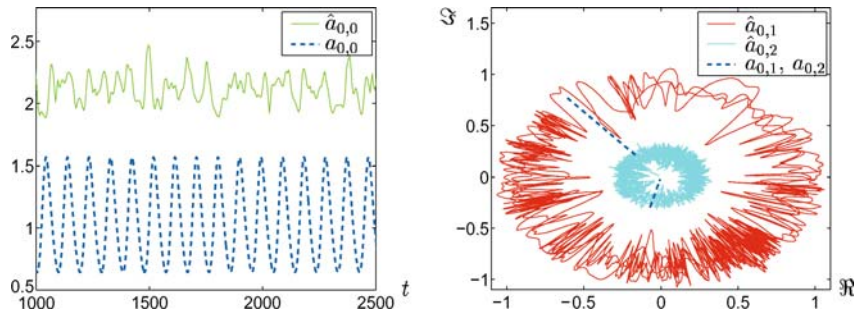


Figure 11. Behaviour of the modified six coupled-mode model compared to the DNS projected onto the (1, 0, 0) (left) and (1, 0, 1), (1, 0, 2) modes (right).

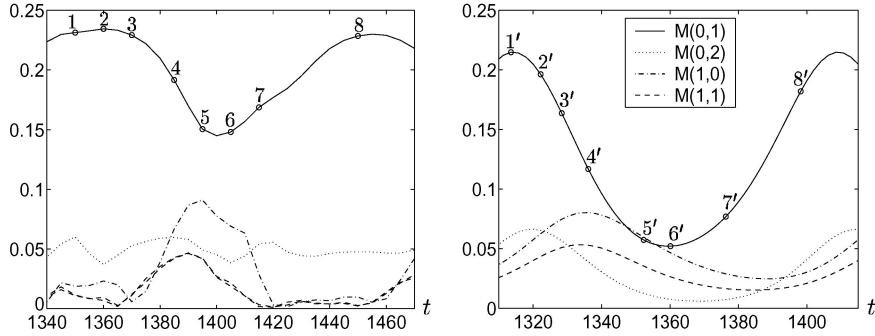


Figure 12. RMS modal velocities: from a representative cycle of the DNS (left) and for one period from the six coupled-mode model, including modelling of losses to neglected modes with $\alpha = 0.8$ (right).

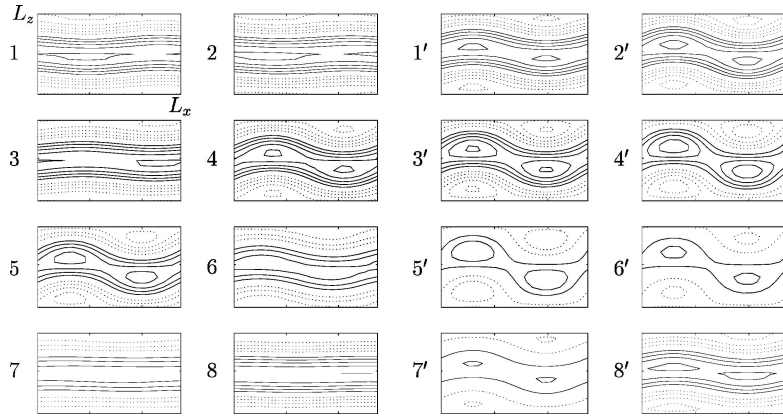


Figure 13. The streak breakdown process viewed in the (x, z) plane lying between the two plates in PCF: DNS projected onto the 6 modes present in the model (left) and computed from one period of the six coupled-mode model (right).

the DNS. The left panels of this figure repeats data from Figure 3, but projected only onto the 6 modes present in the model (so the majority of the small scales in Figure 3 is removed, leaving only large scale structures). Figure 13 confirms that the solution provides reasonable reconstructions of the streak-breakdown process in the (x, z) mid-plane. Reference [46] shows further comparisons between the model and DNS behaviour, including detailed turbulence statistics.

5.2. A NINE UNCOUPLED-MODE MODEL

Uncoupling the $(1, 0, 1)$, $(1, 0, 2)$, $(1, 0, 3)$, $(1, 1, \pm 1)$, and $(1, 1, \pm 2)$ POD modes as outlined in Section 4.3 and projecting Equation (26) onto these modes along with the single-component $(1, 0, 0)$ and $(1, 1, 0)$ POD modes, we obtain ODEs for the following set of sixteen modal amplitudes:

$$(a_{0,0}^{(1)}, a_{0,1}^{(1)[1,2]}, a_{0,2}^{(1)[1,2]}, a_{0,3}^{(1)[1,2]}, a_{1,0}^{(1)}, a_{1,1}^{(1)[1,2]}, a_{1,-1}^{(1)[1,2]}, a_{1,2}^{(1)[1,2]}, a_{1,-2}^{(1)[1,2]}).$$

These equations are quite lengthy, but have similar structure to the coupled equations, with differences in the linear terms which are no longer diagonal; indeed, the linear operator is now non-normal, cf. [5, 6]. We note that $a_{0,0}^{(1)}$ is real, all other modal amplitudes are complex, and that all modes other than $a_{0,0}^{(1)}$ and

$a_{1,0}^{(1)}$ appear in pairs. Counting each complex mode as two real dimensions, this nine uncoupled-mode model is therefore 31-dimensional.

In contrast to the coupled-mode model described above, appropriate modelling of the losses to neglected modes renders the laminar state stable for all Reynolds numbers; indeed, when such modelling is added, solutions started sufficiently close to this laminar state approach it as $t \rightarrow \infty$. However, at $Re = 400$ almost all initial conditions of significant amplitude approach a periodic orbit. This is consistent with the observation that the MFU turbulent state appears as the Reynolds numbers passes between 300 and 400 (cf. [22]).

RMS modal velocities for this model, calculated via an analogue of (103), are compared with the same quantities for DNS in Figure 14. Whilst magnitudes agree fairly well, phase relationships among the model's modal velocities are incorrect; in particular, $M(0, 1)$ and $M(1, 0)$ are now *in phase* and the model streak-breakdown process is consequently phase-shifted, as shown in Figure 15. Nonetheless, the regeneration cycle is reproduced reasonably well.

In addition to this periodic orbit, there are many other periodic and stationary states; some of the latter are shown in Figure 16. These are generated in saddle-node bifurcations, predominantly in the range $Re = 200-375$, and most are unstable. These branches are qualitatively similar to those found

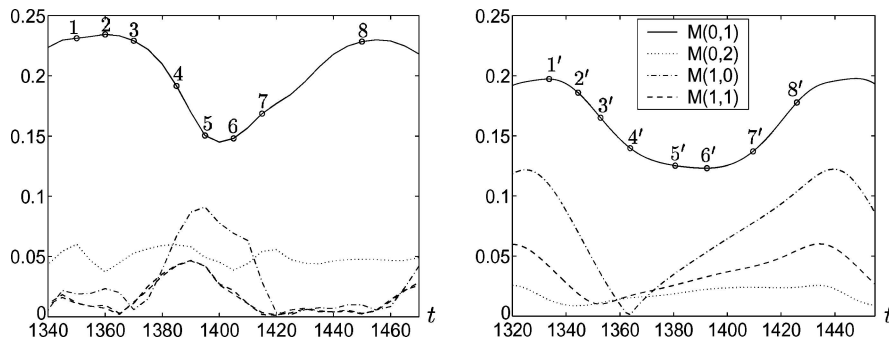


Figure 14. RMS modal velocities: from a representative cycle of the DNS (left) and computed from one period of the nine uncoupled-mode model (right).

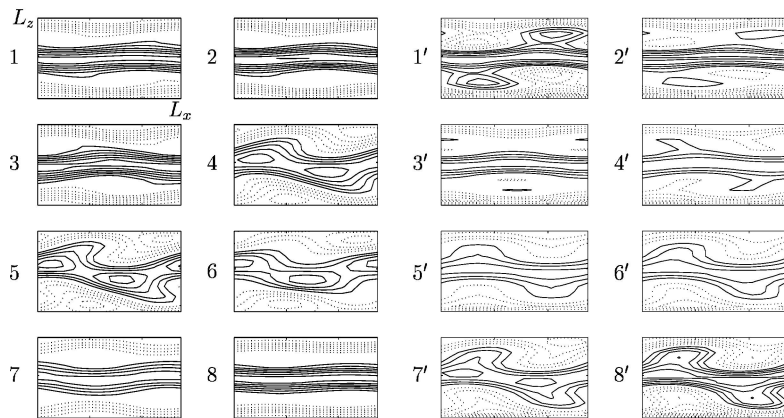


Figure 15. The streak breakdown process as viewed in the (x, z) plane lying between the two plates in PCF: DNS projected onto the 9 modes present in the model (left) and computed from one period of the nine uncoupled-mode model (right).

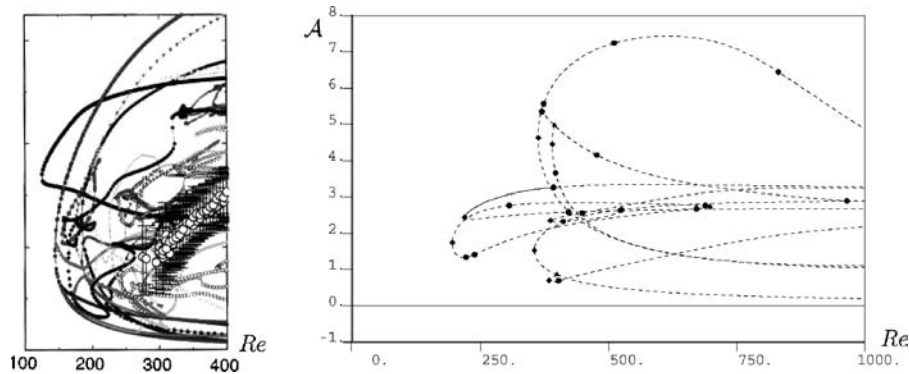


Figure 16. Branches of fixed points in PCF with $L_x = 4\pi$ and $L_z = 2\pi$, from [41] with minor modifications (left). Branches of fixed points in the full phase space of the nine uncoupled-mode model with $\alpha = 0.22$; the ordinate \mathcal{A} denotes the L^2 norm and the stable laminar solution is represented by the solid line at $\mathcal{A} = 0$ (right). Solid (resp., dashed) lines indicate stable (resp., unstable) solutions, and the dots indicate bifurcation points.

by Schmiegel [41] for the full Navier Stokes equations, albeit in a larger domain; also see [13, 37]. Decoupling the modes, along with modeling to represent losses to neglected modes, restores the correct stability type to the trivial laminar flow solution over the full Re range as well as retaining much of the quantitative behaviour of the regeneration cycle at $Re = 400$, and revealing branches of fixed points and periodic orbits similar to those found by these direct computations on the steady NSE.

6. Conclusions

In this paper, we have described how the proper orthogonal decomposition (POD) can be used to construct low-dimensional ordinary differential equation models for fluid flows. Specifically, the POD identifies empirical eigenfunctions (“POD modes”) which optimally capture average energy content from experimental or numerical data. By projecting the evolution partial differential equations for a fluid flow onto these modes and then truncating, one obtains low-dimensional ordinary differential equation models for the fluid flow. In addition to providing a general overview of this procedure, we also described two different ways to numerically calculate the POD modes, discussed how one can exploit symmetry considerations to simplify and understand such modes, commented on how parameter variations are captured naturally in such models, and included a discussion of a generalization of the typical procedure for deriving such models, namely the projection onto uncoupled modes which allow streamwise and cross-stream components to evolve independently, restoring degrees of freedom that are constrained in very low-dimensional truncations.

We then illustrated this procedure for the example of plane Couette flow in a Minimal Flow Unit – a domain whose spanwise and streamwise extent is just sufficient to maintain turbulence. This is an instructive example because the geometry is simple, but exhibits both continuous and discrete symmetries. Drawing upon [46], we summarized the behaviour of two low-dimensional models for this flow, with one involving coupled POD modes and the other uncoupled POD modes. We believe that our attempts to model plane Couette flow in the Minimal Flow Unit are a partial success, and that our detailed comparisons to DNS data (cf. [46]) demonstrate the promise of this procedure for other fluid flows. However, we qualify this by emphasising that this procedure is not entirely straightforward; in particular the best model is not necessarily obtained by keeping the most energetic modes. Indeed, while

the POD necessarily yields sets of modes that contain the majority of the average turbulent kinetic energy, it is a rather poor indicator of which modes are *essential to the dynamics*. Despite this, through judicious selection of model truncations and appropriate modelling of losses to neglected modes, one may use this technique to construct convincing low-dimensional ODEs models, the components (amplitudes and coefficients) of which derive directly from the Navier Stokes equations.

We close by mentioning a few extensions of the proper orthogonal decomposition which may lead to improved models for some fluid systems. The method of Rowley and Marsden [40] was proposed for the low-dimensional modelling of systems with translational symmetry. The procedure relies on an examination of the data in a frame which moves along with travelling structures, the application of the POD-Galerkin technique to data in this frame, and the formation of a reconstruction equation to describe the evolution of these structures in the inertial frame. An extension of this procedure for systems with self-similar solutions was recently proposed in [39]. Another interesting variant of the standard POD-Galerkin method was proposed by Kwasniok [29–31], in which the dynamical features of the governing PDE are taken into account in the construction of a low-dimensional model. In [29], it is proposed that a set of spatial structures could be obtained by minimising the error in the time derivative between the PDE and the reduced order model in a mean least squares sense. In [30], an alternative method is proposed in which the time evolution of the governing PDE and reduced system are minimised over finite time interval. This problem may be formulated as a variational principle and then solved using techniques from the field of optimal control. Here the standard POD basis falls out as a limiting case, where the time interval of interest is reduced to zero. In the two papers [31, 30], Kwasniok shows that the method can be used to construct low-dimensional models of one-dimensional PDEs such as the KSE and Ginzberg–Landau equation, with approximately 40% fewer modes than would be required with the standard POD.

Acknowledgements

This work was supported by DoE: DE-FG02-95ER25238 (T.S. and P.H.) and a National Science Foundation Mathematical Sciences Postdoctoral Research Fellowship to J.M. We thank Clancy Rowley for allowing the use, and modification, of his channel flow code.

References

1. Anderson, E., Bai, Z., Bischof, C., Blackford, S., Demmel, J., Dongarra, J., Croz, D. J., Greenbaum, A., Hammarling, S., McKenney, A., and Sorenson, D., *LAPACK User's Guide, Third Edition*, Society for Industrial and Applied Mathematics, Philadelphia, PA, 1999.
2. Aubry, N., 'A Dynamical System/Coherent Structure Approach to the Fully Developed Turbulent Wall Layer', PhD thesis, Cornell University, 1987.
3. Aubry, N., Holmes, P., Lumley, J. L., and Stone, E., 'The dynamics of coherent structures in the wall region of the turbulent boundary layer', *Journal of Fluid Mechanics* **192**, 1988, 115–173.
4. Aubry, N., Lian, W.-Y., and Titi, E. S., 'Preserving symmetries in the proper orthogonal decomposition', *SIAM Journal on Scientific Computing* **14**, 1993, 483–505.
5. Baggett, J. S., Driscoll, T. A., and Trefethen, L. N., 'A mostly linear model of transition to turbulence', *Physics of Fluids* **7**, 1995, 833–838.
6. Baggett, J. S. and Trefethen, L. N., 'Low-dimensional models of subcritical transition to turbulence', *Physics of Fluids* **9**, 1997, 1043–1053.
7. Bech, K. H., Tillmark, N., Alfredsson, P. H., and Andersson, H. I., 'An investigation of turbulent plane Couette flow at low Reynolds numbers', *Journal of Fluid Mechanics* **286**, 1995, 291–325.

8. Berkooz, G., Holmes, P., and Lumley, J. L., 'Intermittent dynamics in simple models of the wall layer', *Journal Fluid Mechanics* **230**, 1991, 75–95.
9. Berkooz, G., Holmes, P., and Lumley, J. L., 'The proper orthogonal decomposition in the analysis of turbulent flows', *Annual Review of Fluid Mechanics* **25**, 1993, 539–575.
10. Berkooz, G. and Titi, E. S., 'Galerkin projections and the proper orthogonal decomposition for equivariant equations', *Physics Letters A* **174**, 1993, 94–102.
11. Brown, G. L. and Roshko, A., 'On density effects and large structures in turbulent mixing layers', *Journal Fluid Mechanics* **64**, 1974, 775–816.
12. Chossat, P. and Lauterbach, R., *Methods in Equivariant Bifurcations and Dynamical Systems*, World Scientific, Singapore, 2000.
13. Clever, R. M. and Busse, F. H., 'Three-dimensional convection in a horizontal fluid layer subjected to a constant shear', *Journal of Fluid Mechanics* **234**, 1992, 511–527.
14. Crawford, J. D. and Knobloch, E., 'Symmetry and symmetry-breaking bifurcations in fluid mechanics', *Annual Review of Fluid Mechanics* **23**, 1991, 341–387.
15. Dauchot, O. and Daviaud, F., 'Finite amplitude perturbation and spots growth mechanism in plane Couette flow', *Physics of Fluids* **7**(2), 1995, 335–343.
16. Dauchot, O. and Daviaud, F., 'Streamwise vortices in plane Couette flow', *Physics of Fluids* **7**, 1995, 901–903.
17. Dellnitz, M., Golubitsky, M., and Nicol, M., 'Symmetry of attractors and the Karhunen-Loève decomposition', in *Trends and Perspectives in Applied Mathematics*, L. Sirovich (ed.), Springer-Verlag, Berlin, 1994, pp. 73–108.
18. Drazin, P. G. and Reid, W. H., *Hydrodynamic Stability*, Cambridge University Press, Cambridge, UK, 1981.
19. Gibson, J., 'Dynamical Systems Models of Wall-Bounded, Shear-Flow Turbulence', PhD thesis, Cornell University, 2002.
20. Golubitsky, M. and Stewart, I., *The Symmetry Perspective*, Birkhauser Verlag, Basel, 2002.
21. Golubitsky, M., Stewart, I., and Schaeffer, D. G., *Singularities and Groups in Bifurcation Theory*, Vol. II, Springer-Verlag, New York, 1988.
22. Hamilton, J., Kim, J., and Waleffe, F., 'Regeneration mechanisms of near-wall turbulence structures', *Journal of Fluid Mechanics* **287**, 1995, 317–348.
23. Herzog, S., 'The Large Scale Structure in the Near Wall Region of a Turbulent Pipe Flow', PhD thesis, Cornell University, 1986.
24. Holmes, P., 'Can dynamical systems approach turbulence?' in *Whither Turbulence? Turbulence at the Crossroads*, J. L. Lumley (ed.), Springer-Verlag, New York, 1990, pp. 195–249.
25. Holmes, P., Lumley, J. L., and Berkooz, G., *Turbulence, Coherent Structures, Dynamical Systems and Symmetry*, Cambridge University Press, Cambridge, UK, 1996.
26. Holmes, P., Lumley, J. L., Berkooz, G., Mattingly, J. C., and Wittenberg, R. W., 'Low-dimensional models of coherent structures in turbulence', *Physics of Reports* **287**, 1997, 337–384.
27. Kline, S. J., 'The structure of turbulent boundary layers', *Journal of Fluid Mechanics* **30**, 1967, 741–173.
28. Komminaho, J., Lundbladh, A., and Johansson, A. V., 'Very large structures in plane turbulent Couette flow', *Journal of Fluid Mechanics* **320**, 1996, 259–285.
29. Kwasniok, F., 'The reduction of complex dynamical systems using principal interaction patterns', *Physica D* **92**, 1996, 28–60.
30. Kwasniok, F., 'Optimal Galerkin approximations of partial differential equations using principal interaction patterns', *Physical Review E* **55**, 1997, 5365–5375.
31. Kwasniok, F., 'Low-dimensional models of the Ginzburg–Landau equation', *SIAM Journal of Applied Mathematics* **61**, 2001, 2063–2079.
32. Lomont, J. S., *Applications of Finite Groups*, Dover, New York, 1993.
33. Lumley, J. L., 'The structure of inhomogeneous turbulence', in *Atmospheric Turbulence and Wave Propagation*, A. M. Yaglom and V. I. Tatarski (eds.), Nauka, Moscow, 1967, pp. 166–78.
34. Moehlis, J., Smith, T. R., Holmes, P., and Faisst, H., 'Models for turbulent plane Couette flow using the proper orthogonal decomposition', *Physics of Fluids* **14**(7), 2002, 2493–2507.
35. Moffatt, H. K., 'Fixed points of turbulent dynamical systems and suppression of nonlinearity', in *Whither Turbulence? Turbulence at the Crossroads*, J. L. Lumley (ed.), pp. 250–257. Springer-Verlag, New York, 1990.
36. Moin, P. and Moser, R. D., 'Characteristic-eddy decomposition of turbulence in a channel', *Journal of Fluid Mechanics* **200**, 1989, 471–509.
37. Nagata, M., 'Three-dimensional finite-amplitude solutions in plane Couette flow: Bifurcation from infinity', *Journal of Fluid Mechanics* **217**, 1990, 519–527.
38. Rowley, C. W., Colonius, T., and Murray, R. M., 'Dynamical models for control of cavity oscillations', *AIAA Paper 2001–2126*, 2001, pp. 2126–2134.
39. Rowley, C. W., Kevrekidis, I., Marsden, J., and Lust, K., 'Reduction and reconstruction for self-similar dynamical systems', *Nonlinearity* **16**, 2003, 1257–1275.
40. Rowley, C. W. and Marsden, J. E., 'Reconstruction equations and the Karhunen-Loève expansion for systems with symmetry', *Physica D* **142**, 2000, 1–19.

41. Schmiegel, A., 'Transition to Turbulence in Linearly Stable Shear Flows', PhD thesis, Universität Marburg, 1999.
42. Sirovich, L., 'Turbulence and the dynamics of coherent structures, parts I–III', *Quarterly Applied Mathematics* **XLV**(3), 1987, 561–582.
43. Smaoui, N. and Armbruster, D., 'Symmetry and the Karhunen–Loève analysis', *SIAM Journal of Scientific Computation* **18**, 1997, 1526–1532.
44. Smith, T. and Holmes, P., 'Low dimensional models with varying parameters: A model problem and flow through a diffuser with variable angle', in *Fluid Mechanics and the Environment: Dynamical Approaches*, J. L. Lumley (ed.), Vol. 566 of Lecture Notes in Physics, Springer-Verlag, New York, 2001, pp. 315–336.
45. Smith, T. R., 'Low-dimensional Models of Plane Couette Flow using the Proper Orthogonal Decomposition', PhD thesis, Princeton University, 2003.
46. Smith, T. R., Moehlis, J., and Holmes, P., 'Low-dimensional models for turbulent plane Couette flow in a minimal flow unit', to appear in *Journal of Fluid Mechanics*.
47. Tennekes, H. and Lumley, J. L., *A First Course in Turbulence*. MIT Press, Cambridge, MA, 1972.
48. Waleffe, F., 'Transition in shear flows. Nonlinear normality versus non-normal linearity', *Physics of Fluids* **7**(12), 1995, 3060–3066.